Energetic Requirements for Dynamos in the Metallic Cores of Super-Earth and Super-Venus Exoplanets

C. H. Blaske[1,2], J. G. O'Rourke[2]

[1]Barrett, The Honors College, Arizona State University, Tempe AZ

[2]School of Earth and Space Exploration, Arizona State University, Tempe AZ

Corresponding author: J. G. O'Rourke (jgorourk@asu.edu)

Key Points:

- Super-Earth and super-Venus exoplanets can have Earth-like bulk compositions but surface conditions that are Earth- or Venus-like
- We calculated how fast their metallic cores must cool to sustain a dynamo powered by thermal or chemical convection
- Massive Earth- and Venus-analogues may both host dynamos and potentially detectable magnetospheres if their silicate mantles are solid

Abstract

Super-Earth and super-Venus exoplanets may have similar bulk compositions but dichotomous surface conditions and mantle dynamics. Vigorous convection within their metallic cores may produce dynamos and thus magnetospheres if the total heat flow out of the core exceeds a critical value. Earth has a core-hosted dynamo because plate tectonics cools the core relatively rapidly. In contrast, Venus has no dynamo and its deep interior probably cools slowly. Here we develop scaling laws for how planetary mass affects the minimum heat flow required to sustain both thermal and chemical convection, which we compare to a simple model for the actual heat flow conveyed by solid-state mantle convection. We found that the required heat flows increase with planetary mass (to a power of ~0.8–0.9), but the actual heat flow may increase even faster (to a power of ~1.6). Massive super-Earths are likely to host a dynamo in their metallic cores if their silicate mantles are entirely solid. Super-Venuses with relatively slow mantle convection could host a dynamo if their mass exceeds ~1.5 (with an inner core) or ~4 (without an inner core) Earth-masses. However, the mantles of massive rocky exoplanets might not be completely solid. Basal magma oceans may reduce the heat flow across the core-mantle boundary and smother any core-hosted dynamo. Detecting a magnetosphere at an Earth-mass planet probably signals Earth-like geodynamics. In contrast, magnetic fields may not reliably reveal if a massive exoplanet is a super-Earth or a super-Venus. We eagerly await direct observations in the next few decades.

Plain Language Summary

Earth is the largest planet in our Solar System chiefly composed of silicates and metal. However, we now know that so-called Super-Earths—made of rock and metal in Earth-like proportions but with larger masses—are common in our galaxy. No one knows if their surfaces are habitable like Earth or hellish like Venus. In other words, many "super-Earths" might be better described as super-Venuses. Earth's magnetosphere, which has survived for billions of years, is perhaps a symptom of habitability. Without our liquid water oceans and mild temperatures, Earth might not have plate tectonics, which cools Earth's rocky mantle and metallic core relatively quickly. In contrast, Venus may lack a dynamo because its core cools slowly. Detecting any magnetic field from rocky exoplanets may become possible in a few decades. Would such a detection prove that a super-Earth is a true Earth-analogue? Here we calculate the minimum heat flow out of massive metallic cores required to sustain a dynamo under different circumstances. We compare these

thresholds to a simple model of the actual heat flow. We find that a super-Earth without a magnetic field is probably not a scaled-up Earth. However, massive Venus-analogues with inner cores may also host magnetic fields.

1 Introduction

Thousands of exoplanets have been discovered since the Kepler Space Telescope was launched in 2009, and the pace of discovery is only increasing. Exoplanets with an Earth-like density but a mass between ~1 and 10 Earth-masses (M_E) are often collectively called super-Earths. Observationally, exoplanets with radii larger than ~1.5 Earth-radii (≥5 M_E) mostly have low densities, implying that they acquired thick, volatile envelopes and are perhaps "mini-Neptunes" (e.g., Rogers, 2015; Weiss & Marcy, 2014). However, some >5-M_E super-Earths probably exist even if they are statistically rare. It cannot be overemphasized that a super-Earth may not have Earth-like surface conditions (e.g., Tasker et al., 2017). For example, the bulk densities of Venus and Earth are similar but the surface of Venus is a hellish wasteland (e.g., Kane et al., 2019). No super-Earth exoplanet is yet distinguishable from a massive Venus-analogue (e.g., Foley et al., 2012; Foley & Driscoll, 2016; Kane et al., 2014), a "super-Venus" (e.g., Kane et al., 2013). Super-Earths (and super-Venuses) are interesting as individual worlds—and they allow us to study how planetary mass affects planetary evolution.

Magnetic fields may open unique windows into the internal structure and dynamics of super-Earths. Magnetospheres have complex effects on atmospheric loss processes over time (e.g., Dong et al., 2020). The direct impact of planetary magnetism on habitability is debated (e.g., Driscoll, 2018). However, detecting a magnetic field may indirectly constrain the habitability of the surface. Terrestrial planetary bodies in our Solar System (e.g., Mercury, Venus, Earth, Earth's Moon, and Mars) are differentiated into silicate mantles and metallic cores. All of these bodies, possibly excepting Venus, have global magnetic fields produced by dynamos in their metallic cores now or had such fields in the past (e.g., Stevenson, 2003, 2010). Ultimately, vigorous convection in cores—driven by the loss of heat to the mantle—produces dynamos. Earth and Venus are the same size but Earth has plate tectonics, which cools the deep interior relatively quickly and thus helps drive a dynamo. Surface water and clement temperatures are possibly expected to help initialize and sustain plate tectonics (e.g., Bercovici & Ricard, 2014; Korenaga, 2012), and thus improve the likelihood of a long-lived magnetosphere.

However, our Solar System provides too small of a sample size to understand all factors that affect a dynamo.

The purpose of this study is to determine how the likelihood that an exoplanet hosts a dynamo in its metallic core changes with planetary mass. Recent studies provide detailed models for the internal structures of massive rocky planets (e.g., Boujibar et al., 2020; Noack & Lasbleis, 2020; Unterborn & Panero, 2019). Here we use thermodynamics to calculate if a dynamo may exist given the overall cooling rate of the metallic core. We assume that the core of an Earth-analogue cools quickly compared to the core of a Venus-analogue as a consequence of their different mantle dynamics, which we do not model in detail. In other words, a 1-M_E Earth-analogue is cooling fast enough to support a dynamo, while a 1-M_E Venus-analogue does not have enough power in the core. The actual heat flux out of Earth's core is uncertain between ~5–15 TW (e.g., Lay et al., 2008). Most models of Venus feature a total heat flux out of the core of <5 TW (e.g., Nimmo, 2002; O'Rourke et al., 2018). However, we do not know the actual heat flux for Venus—or even whether its core is fully or partially liquid (e.g., Dumoulin et al., 2017). In our study, Earth- and Venus-analogues both have well-mixed cores with identical structures and compositions. However, Jacobson et al. (2017) proposed that Earth's core is well-mixed but the core of Venus is chemically stratified because Venus experienced a gentle accretion without a late energetic impact. Ultimately, our simplifying assumptions guarantee that a super-Earth is more likely to host a dynamo than a super-Venus. We address whether super-Earths and super-Venuses are more likely to host a dynamo than Earth and Venus, respectively.

Some previous studies suggested that super-Earths are unlikely to host a dynamo regardless of surface conditions and the mode of mantle dynamics. For example, Gaidos et al. (2010) asserted that cores in planets more massive than ~2–3 Earth-masses do not crystallize from the middle outwards, meaning that an inner core would never nucleate. Earth's inner core is a dominant source of power for our dynamo today (e.g., Labrosse, 2015; Nimmo, 2015)—the absence of an inner core in super-Earths would reduce the longevity of any dynamo. Relatedly, Tachinami et al. (2011) assumed that the mantles of super-Earths above ~2–3 Earth-masses are incredibly viscous, which leads to elevated temperatures in the lower mantle and thus a tiny thermal contrast across the core-mantle boundary (CMB). Shallow thermal gradients at the CMB translate into low heat flow, which implies that the metallic core would cool via thermal conduction without the vigorous fluid motions that are required to produce a dynamo. However, the mineral physics assumed in these studies contrasts with some recent work.

Recent work predicts that super-Earths are in fact likely to support dynamos, especially if they are true Earth-analogues (e.g., Boujibar et al., 2020; Driscoll & Olson, 2011). An inner core is not always necessary to generate a magnetic field. Indeed, Earth's inner core may not have existed for most of our dynamo's lifetime (e.g., Bono et al., 2019; Labrosse, 2015). Driscoll & Olson (2011) determined that thermal convection alone can produce magnetic fields on the surfaces of super-Earths that are twice as strong as Earth's surface field—if their mantle dynamics efficiently cool the metallic core. Indeed, the viscosity of silicates in the lower mantles of super-Earths is highly uncertain but might not be much higher than in Earth's lower mantle (e.g., Karato, 2011; Stamenković et al., 2012). Van Summeren et al. (2013) found that massive Earth-analogues (i.e., with plate tectonics) could have strong dynamos that persist for billions of years powered by either thermal or compositional convection. In contrast, massive Venus-analogues (i.e., without plate tectonics) would only have (weak) dynamos once an inner core crystallized and kickstarted compositional convection. Crucially, Boujibar et al. (2020) found that state-of-the-art equations of state for iron alloys imply that metallic cores of super-Earths should crystallize from the center outwards—forming an inner core. The temperature range over which a super-Earth hosts an inner core expands as planetary mass increases, meaning that massive exoplanets may likely have inner cores.

2 Theory and Numerical Methods

Our three-step approach provides the energetic requirements for dynamos in the metallic cores of super-Earths. First, we derive the radial profiles of density and pressure in the core. We consider planets with masses from 1 to 10 Earth-masses (M_E) in increments of 1 M_E. As in Earth, the mass of the core equals 32.5% of the planetary mass. We integrate the fundamental equations of planetary structure to obtain self-consistent descriptions of the internal structure. Second, we fit those radial profiles to polynomial equations that are amenable to analytic manipulations. These equations are used to parameterize the different sources and sinks of energy in the core.

Third, we calculate three different thresholds (Q_{ad}, Q_{noIC}, and Q_{yesIC}) for the critical heat flow required for a dynamo. The highest threshold is the adiabatic heat flow (Q_{ad}), which is what thermal conduction would transport up an isentropic gradient in the core—called the adiabat because it represents how fluid parcels cool as they rise without exchanging heat with their surroundings. Radiogenic heat and chemical buoyancy from the precipitation of light elements at the core/mantle boundary can reduce the critical heat flow to a lower value (Q_{noIC}). The lowest threshold (Q_{yesIC}) is applicable if a growing inner core helps power convection.

The following sub-sections describe our approach. Foundational references include Boujibar et al. (2020), Labrosse (2015), and O'Rourke (2020). Figure 1 shows the critical parameters that define the structure and evolution of the core. Table 1 lists the constants derived for cores with different masses. Table 2 defines the variables that are calculated to describe the energetics and thermochemical evolution of the core.

2.1 Structure of planetary cores

Our first task is to discover how density and pressure vary with depth within the metallic cores of super-Earths with different masses. For any planetary body, the general approach is to integrate three equations (e.g., Boujibar et al., 2020; Seager et al., 2007; Sotin et al., 2007; Unterborn & Panero, 2019; Valencia et al., 2006). First, we consider the definition of mass:

$$\frac{dm}{dr} = 4\pi r^2 \rho. \tag{1}$$

Here $m(r)$ is the mass enclosed inside a sphere with radius r and density ρ. Pressure (P) increases with depth according to hydrostatic equilibrium:

$$\frac{dP}{dr} = -\rho g. \tag{2}$$

Gravitational acceleration is calculated as $g(r) = Gm(r)/r^2$, where G is the gravitational constant. Finally, we use a Vinet equation of state for liquid iron to relate P and ρ (Boujibar et al., 2020):

$$P = 3K_{0V}\eta^{\frac{2}{3}}\left(1-\eta^{-\frac{1}{3}}\right)\exp\left[\frac{3}{2}(K_{1V}-1)\left(1-\eta^{-\frac{1}{3}}\right)\right]. \tag{3}$$

Here K_{0V} = 125 GPa and K_{1V} = 5.5 are the bulk modulus and its pressure-derivative, respectively, and $\eta = \rho/\rho_{0V}$ is the ratio of density (ρ) to a zero-pressure density (ρ_{0V} = 7700 kg/m^3). These parameters are consistent with recent experiments on an iron-sulfur alloy with ~7 wt% Si (Wicks et al., 2018). We ignore the effects of temperature on the equation of state.

We use an iterative method to obtain a self-consistent structure. First, we guess $P(0)$, the pressure at the center of the core. We numerically integrate Eq. 1–3 starting at the center in radial increments of 1 km. As radius increases, P decreases and $m(r)$ increases. The outer boundary of the core is reached when $m(R_C) = 0.325M_P$, where R_C is the radius of the core and M_P is the mass of the planet. Unterborn & Panero (2019) found that the pressure at the CMB equals

$$P(R_C) = 1\ \text{GPa}\left[262\left(\frac{\mathrm{R_P}}{R_E}\right) - 550\left(\frac{R_P}{R_E}\right)^2 + 432\left(\frac{R_P}{R_E}\right)^3\right]. \tag{4}$$

Here R_P is the radius of the planet and R_E is Earth's radius, where $R_P = R_E(M_P/M_E)^{0.27}$ (Valencia et al., 2006). We use the bisection method to adjust our guess for $P(0)$ until our value of $P(R_C)$ agrees with Equation 4 within 0.05%.

Once the basics of the internal structure are determined, we calculate other key thermodynamic properties. The Grüneisen parameter and the coefficient of thermal expansion vary with depth as $\gamma(r) = 1.6\eta^{0.92}$ and $\alpha(r) = (4 \times 10^{-6}\ \mathrm{K}^{-1})\eta^{-3}$, respectively (Boujibar et al., 2020). We take the volume-averaged values of $\gamma(r)$ and $\alpha(r)$ as representative of the entire core. Next, the liquidus (melting) temperature at the center of the core is $T_L(0) = (5800\ \mathrm{K})[P(0)/(423\ \mathrm{GPa})]^{0.515}$ and its pressure-derivative is $\mathrm{d}T_L/\mathrm{d}P = (9\ \mathrm{K\ GPa^{-1}})[P(0)/(423\ \mathrm{GPa})]^{-0.485}$ (Boujibar et al., 2020; Stixrude, 2014). This liquidus is valid for cores containing several wt% of impurities.

Finally, we formulate parameterizations of density and temperature that are convenient to use in the rest of our model. The radial profile for density is fit to a fourth-order polynomial:

$$\rho(r) = \rho_0\left[1 - \left(\frac{r}{L_\rho}\right)^2 - A_\rho\left(\frac{r}{L_\rho}\right)^4\right], \tag{5}$$

where L_ρ is a length scale and A_ρ is a fitting constant (Labrosse, 2015). To quantify how density changes with pressure, we define an effective bulk modulus as $K_0 = 2\pi G(L_\rho\rho_0)^2/3$ and its derivative as $K_1 = (10A_\rho + 13)/5$. Note that K_0 and K_1 are not the same as the K_{0V} and K_{1V} used in the equation of state (Eq. 3), despite their identical dimensions. We assume an adiabatic thermal gradient in the outer core, so $T(r) = T(0)[\rho(r)/\rho_0]^\gamma$.

2.2 Energy budget for the core

A dynamo may exist if there is enough energy in the outer core to power vigorous convection. We assume the planetary rotation rate is fast enough for the Coriolis force to organize convective flow in the core (e.g., Stevenson, 2003, 2010). Either thermal or chemical buoyancy can provoke convection. Thermal convection occurs when hot material rises while cold material sinks. Chemical reactions can add or remove light elements from the iron alloy, providing chemical buoyancy that can augment thermal buoyancy or compensate for its absence. Our approach to assessing the energy budget follows many previous studies (e.g., Labrosse, 2015; Nimmo, 2015a, 2015b). The most important parameter is the total heat flow across the core-mantle boundary (Q_{CMB}), which must exceed a critical value to drive convection and thus a dynamo. Mantle dynamics control Q_{CMB} based on how fast solid-state convection in the mantle transports heat upwards from its lower boundary. Detailed simulations of mantle dynamics are complex, uncertain, and beyond the scope of this study. Our goal is to determine how large Q_{CMB} must be to sustain a dynamo. In the core, Q_{CMB} is partitioned into six individual energy sources:

$$Q_{CMB} = Q_S + Q_R + Q_P + Q_G + Q_L + Q_I. \tag{6}$$

Exact formulas for all terms on the right side of this equation are found in the Supporting Information, which are mostly based on (but use different notation than) Labrosse (2015). Those formulas are unwieldy polynomials derived by integrating the density and temperature profiles over the volume of the outer core. Rather than wallow in the gory details, we explain the meaning of each term and how they relate to thermodynamic properties of the core.

The first three terms in Eq. 6 are important regardless of whether an inner core exists. First, Q_S represents the secular cooling of the outer core. This term equals the product of the specific heat of the outer core, its total mass, and the rate at which its temperature decreases ($\mathrm{d}T_C/\mathrm{d}t$). Second, Q_R is radiogenic heating in the outer core. Potassium is probably the primary source of radiogenic heating, but uranium and thorium may contribute additional heating (e.g., Blanchard et al., 2017; Chidester et al., 2017). We assume potassium is incompatible in solid iron, so its concentration in the outer core increases as the inner core grows. Hirose et al. (2013) argued that [K] < 50 ppm (our nominal value) for Earth, but [K] could vary for different exoplanets. Third, Q_P is associated with chemical precipitation at the CMB. Elements such as silicon, oxygen, and magnesium become less soluble in iron alloys at colder temperatures (e.g., Badro et al., 2016, 2018; Du et al., 2019; Hirose et al., 2017). When they precipitate, they move into the lower mantle and leave behind dense fluid. This process releases gravitational energy that promotes chemical convection in the core (e.g., Buffett et al., 2000; O'Rourke & Stevenson, 2016). We assume the mass flux of precipitated material equals a constant multiplied by $\mathrm{d}T_C/\mathrm{d}t$ and the mass of the outer core. Our nominal value for the precipitation rate (P_P) matches that used in recent models of Earth's evolution (Badro et al., 2018; Du et al., 2019; Liu et al., 2019; Mittal et al., 2020). We have not analyzed how P_P may change with increasing planetary mass.

The final three terms in Eq. 6 are related to the inner core. Light elements, especially oxygen, are incompatible in solid iron. As the core freezes from the center outwards, they are excluded from the inner core and create a flux of light material into the base of the outer core. While precipitation at the CMB drives chemical convection from above, Q_G is a gravitational energy term that represents chemical convection driven from below. Crystallization of the inner core also involves latent heat, Q_L. Finally, we assume the inner core has infinite thermal conductivity. Its temperature then equals $T_L(R_I)$, the liquidus temperature at the inner core boundary. The last term in Eq. 6, Q_I, is the heat flux associated with this cooling. The opposite assumption made in some studies is that the inner core is perfectly insulating and $Q_I = 0$ TW (Labrosse, 2015). Either assumption is fine for Earth-like inner core radii ($R_I/R_C \sim 0.3$) where Q_I is <5% of Q_C, although Q_I can be important when R_I is relatively large.

2.3 Dissipation budget for a dynamo in the core

Using the energy budget for the outer core, we calculate the total dissipation available to power a dynamo, Φ. Our models assume a dynamo exists if there is any positive dissipation (i.e., if $\Phi > 0$ W). In reality, the total dissipation must exceed the amount of Ohmic heating caused by the electrical resistance of the core fluid (e.g., Christensen, 2010). Ohmic losses are poorly constrained but could be as large as the adiabatic heat flow (e.g., Stelzer & Jackson, 2013). Our calculations thus provide a lower bound on the energetic requirements for a dynamo. Crucially, an "instantaneous" value for Q_{CMB} is used to calculate Φ because the free decay time for a planetary dynamo is only $\sim 10^4$ years (e.g., Stevenson, 2003, 2010). Various scaling laws are available to convert Φ into the surface intensity of the magnetic field (e.g., Aubert et al., 2009; Landeau et al., 2017). This study is chiefly concerned with the existence (or not) of a dynamo.

Each term in the heat budget has a counterpart in the dissipation budget that is labeled with the same subscript. The dissipation budget is derived from the combination of the energy budget (Eq. 6) and the entropy balance (e.g., Eq. 29 in Labrosse, 2015). Thermal conduction inside the outer core is not part of the energy budget. However, thermal conduction is a sink of entropy and thus appears in the dissipation budget. In total,

$$\Phi = \Phi_S + \Phi_R + \Phi_P + \Phi_G + \Phi_L + \Phi_I - \Phi_K. \quad (7)$$

The key point is that each dissipation term (Φ_i) equals the corresponding energy term (Q_i) multiplied by a dimensionless efficiency factor that depends on whether the energy source is thermal or chemical. Thermal terms (subscripts S, R, L, and I) have "Carnot-like" efficiencies:

$$\Phi_i = \frac{T_D(T_i - T_C)}{T_i T_C} Q_i, \quad (8)$$

where T_D is the average temperature in the core (Figure 1c), T_C is the temperature at the CMB, and T_i is an effective temperature associated with the dissipation of each energy source. Radiogenic heating is uniformly distributed within the outer core so $T_R = T_D$. The effective temperature associated with secular cooling (T_S) is slightly hotter, but typically only by a few degrees. Both T_L and T_I equal $T_L(R_I)$, the temperature at the inner core boundary. These temperatures are defined in the Supporting Information. Compared to thermal buoyancy, chemical effects are very efficient at driving convection. The efficiency factors for Φ_P and Φ_G equal T_D/T_C (i.e., $\Phi_P = [T_D/T_C]Q_P$ and $\Phi_G = [T_D/T_C]Q_P$), which is larger by a factor of ~2–10 than those from Equation 8. The dissipation sink associated with conduction (Φ_K) is directly proportional to T_C and the thermal conductivity of the core (k_C). The full dissipation budget is

$$\Phi = \frac{T_D(T_S - T_C)}{T_S T_C} Q_S + \frac{T_D - T_C}{T_C} Q_R + \frac{T_D}{T_C}(Q_P + Q_G) + \frac{T_D[T_L(R_I) - T_C]}{T_L(R_I) T_C}(Q_L + Q_I) - \Phi_K. \quad (9)$$

Ultimately, thermal terms dominate the heat budget (e.g., $Q_S >> Q_G$) but chemical terms can dominate the dissipation budget (e.g., $\Phi_G >> \Phi_S$).

We use the dissipation budget to calculate the three critical thresholds above which a dynamo may exist. First, the critical heat flow in the presence of an inner core (Q_{yesIC}) is simply the minimum value of Q_{CMB} above which $\Phi > 0$ W according to Eq. 9. Second, the critical heat flow in the absence of an inner core (Q_{noIC}) is calculated by removing Q_G, Q_L, and Q_I from the global heat budget and then solving for Q_{CMB} with Eq. 6 and 9. That analytic equation is included in the Supporting Information. Finally, the adiabatic heat flow (Q_{ad}) is the minimum required to power a dynamo via thermal convection in the absence of power sources other than secular cooling. We calculate Q_{ad} by reducing the global heat budget to $Q_{CMB} = Q_S$ and then solving for Q_{CMB} with Eq. 6 and 9 with all terms except Φ_S and Φ_K equal to zero:

$$Q_{ad} = \frac{T_S T_C}{T_D(T_S - T_C)} \Phi_K \tag{10}$$

As defined in the Supporting Information, Φ_K is directly proportional to thermal conductivity and increases with planetary mass. By Fourier's law, dividing Q_{ad} from Eq. 10 by k_C yields a representative value of the adiabatic temperature gradient. It is not obvious how Q_{ad} should change as the inner core grows. On one hand, Φ_K is integrated over the shrinking volume of the outer core. On the other hand, all the temperatures (T_S, T_C, and T_D) decrease as the core cools. Thermal conductivity is not temperature-dependent in our model. Inner core growth could have a second-order effect: the thermal conductivity of the core could decrease as the inner core grows and light elements are added to the outer core (e.g., Pozzo et al., 2012; Seagle et al., 2013; Zhang et al., 2021). In any case, we know that $Q_{ad} > Q_{noIC} > Q_{yesIC}$ by definition.2.4

Parameterizing the actual cooling rate of the metallic core

Our energetic calculations treat the heat flow across the CMB as a free parameter. However, we want to compare the minimum heat flow required to sustain a dynamo (Q_{yesIC}, Q_{noIC}, and Q_{ad}) to an estimate of Q_{CMB}. In general, convection in the solid-state mantle regulates how fast heat is transported out of the deeper interior. Here we adapt a decades-old model (e.g., Foley & Driscoll, 2016; Stevenson et al., 1983). We assume a thermal boundary layer exists at the base of the solid, convecting mantle (Figure 2). The thermal contrast across that layer (ΔT_{BL}) is the difference between the temperature at the CMB (T_C) and immediately above the boundary layer in the mantle (T_{LM}). The heat flow out of the core then obeys Fourier's law:

$$Q_{CMB} = 4\pi R_C^2 k_M \left(\frac{\Delta T_{BL}}{\delta_{BL}}\right), \tag{11}$$

where k_M is the thermal conductivity of the lower mantle and δ_{BL} is the thickness of the boundary layer. In steady state, δ_{BL} is related to the Rayleigh number:

$$\mathrm{Ra} = \frac{\rho_M g_C \alpha_M \Delta T_{BL} \delta_{BL}^3}{\kappa_M \mu_{BL}}. \tag{12}$$

Here ρ_M, α_M, and κ_M are the density, coefficient of thermal expansion, and thermal diffusivity in the lower mantle, respectively. The average viscosity (μ_{BL}) is evaluated at the average temperature in the boundary layer. Fluid dynamical experiments and simulations show that the layer becomes unstable to convection when $\mathrm{Ra} \sim \mathrm{Ra}_c \sim 10^3$. If $\mathrm{Ra} > \mathrm{Ra}_c$, then the layer breaks away into a rising mantle plume. If $\mathrm{Ra} < \mathrm{Ra}_c$ instead, then the layer continues to grow by thermal conduction. Therefore, the equilibrium thickness of the boundary layer is

$$\delta_{BL} = \left(\frac{\rho_M g_C \alpha_M \Delta T_{BL}}{\kappa_M \mu_{BL} \mathrm{Ra}_c}\right)^{\frac{1}{3}}. \tag{13}$$

Substituting Eq. 13 into Eq. 11 yields the classic formula for the total heat flow:

$$Q_{CMB} = 4\pi R_C^2 k_M \left(\frac{\rho_M g_C \alpha_M}{\kappa_M \mathrm{Ra}_c}\right)^{\frac{1}{3}} \mu_{BL}^{-\frac{1}{3}} \Delta T_{BL}^{\frac{4}{3}}. \tag{14}$$

To determine how Q_{CMB} scales with planetary mass, we analyzed the individual terms that have significant mass-dependence (i.e., everything but 4π and Ra_c). Some of these terms (e.g., R_C and g) are calculated directly in this study, while the rest of the terms are estimated using the existing literature. Ultimately, we seek power-laws for Q_{CMB}, Q_{ad}, Q_{noIC}, and Q_{yesIC}:

$$\frac{Q(M_P)}{Q(M_E)} = \left(\frac{M_P}{M_E}\right)^{\Sigma}, \tag{15}$$

where Σ is a power-law exponent.

3 Results

3.1 Energetic requirements for a dynamo

Figure 3 shows how the inner core radius and the total heat flow across the core-mantle boundary affect the energetics of the core. More heat flow always provides more dissipation for the dynamo (Fig. 3b, 3c, and 3d). The required heat flow for a dynamo gradually increases with planetary mass. The existence of an inner core increases the likelihood of a dynamo, but the energetics are not too sensitive to its exact radius. That is, Q_{ad}, Q_{noIC}, and Q_{yesIC} have very similar values for R_I/R_C between ~0.1 and 0.7 for all planetary masses. Chemical convection driven by inner core growth can occur if $Q_{CMB} > Q_{yesIC}$. For small inner cores ($R_I/R_C < \sim 0.1$), Q_{yesIC} rapidly decreases as R_I increases because the mass flux of light elements from the inner core grows like R_I squared. Because the mass of the inner core grows like R_I cubed, Q_{yesIC} eventually flattens out and then starts to rise gradually. Thermal convection can occur if $Q_{CMB} > Q_{ad}$. Except when the inner core is very large, Q_{ad} increases with planetary mass. When R_I is $>0.8R_C$ (1 and 5 M_E) or $>0.65R_C$ (10 M_E), Q_{ad} starts to decrease because the volume of the outer core shrinks. The total amount of radiogenic heating and the precipitation rate of light elements at the CMB do not depend on the radius of the inner core. Consequentially, Q_{noIC} is offset below Q_{ad} but displays the same dependence on the normalized inner core radius.

The range of values for the total heat flow where chemical but not thermal convection may occur grows wider with increasing planetary mass. For a 1-M_E planet, the difference between Q_{ad} and Q_{yesIC} is ~3 TW, while the difference in a 10-M_E planet is ~19 TW. The total dissipation available for a dynamo (Φ) at a given Q_{CMB} stays approximately constant as planetary mass changes. While Φ at a fixed Q_{CMB} increases slightly from ~1–5 M_E, it decreases from ~5–10 M_E (Fig. S1), resulting in similar dissipation budgets across a spectrum of planetary masses. We did not calculate actual magnetic field strengths. Instead, we focused on the existence or non-existence of a dynamo. We speculate that magnetic fields for planets of various sizes would be similar in strength in the core. However, the surface fields of larger planets could be weaker because mantle thickness increases with planetary size.

As planetary mass increases, vastly more heat flow is required to change the temperature of the core or to increase the radius of the inner core. For example, the value of $\mathrm{d}T_C/\mathrm{d}t$ associated with a given Q_{CMB} decreases by a factor of ~7 as planetary mass increases from ~1–5 M_E and then decreases again by another factor of ~2 from ~5–10 M_E. The growth rate of the inner core also decreases drastically as planet mass increases. For a 1-M_E planet, $\mathrm{d}R_I/\mathrm{d}t \sim 1$ km/Myr when $R_I/R_C \sim 0.5$ and $Q_{CMB} \sim 40$ TW. For those same values of R_I/R_C and Q_{CMB}, the inner core growth rate is <200 and <50 m/Myr at 5 and 10 M_E, respectively. This result means that massive cores will cool down very slowly over time. Relative to Earth and/or Venus, massive cores may take much longer to solidify (e.g., Boujibar et al., 2020). Thermal evolution models are required to quantify these important timescales (e.g., Bonati et al., 2020).

Table 3 lists representative values of all three critical heat flows for all planetary masses. Figures S1, S2, S3, and S4 illustrate the energetic regime diagrams for all ten planetary masses. We extracted values at $R_I/R_C = 0.3R_C$ as noted in Fig. 3, which are representative of a wide range of inner core radii ($R_I/R_C \sim 0.1$–0.7). We fit each column of values to power laws (Eq. 15) using the least-squares method and report the best-fit exponent and its standard deviation. The first column uses our nominal parameters: [K] = 50 ppm, $P_P = 5 \times 10^{-6}$ 1/K, and $k_C = 40$ W/m/K. The other three columns adjust each parameter individually to determine the sensitivity of our model. As we increase [K], Q_{ad} does not change. Both Q_{yesIC} and Q_{noIC} increase with [K] because thermal convection is less efficient than chemical convection. Raising the proportion of radiogenic heating in the energy budget decreases the dissipation available for a dynamo at a constant total heat flow. Increasing k_C increases Q_{ad}, Q_{noIC}, and Q_{yesIC} because Φ_K feeds into the definition of all three values. Planets of 5 Earth-masses see Q_{ad} increase from ~22–55 TW and Q_{yesIC} increase from ~10– 24 TW as k_C increases from 40 to 100 W/m/K. By definition, changing the precipitation rate of light elements at the CMB does not change Q_{ad} at all. Likewise, Q_{yesIC} is not sensitive to the precipitation rate as long as an inner core exists with $R_I > \sim 0.05R_C$ (Fig. S4). That is, Q_G and Q_P are "substitute goods" in the dissipation budget. If Q_{CMB} is constant, then decreasing Q_P by adjusting P_P simply leads to a larger Q_G (i.e., a faster-growing inner core). Precipitation of light elements at the CMB decreases the energetic requirement for a dynamo by ~25% when there is no inner core. For example, for a 5-M_E planet with $T_C = T_C(0) + 1$ K, Q_{CMB} must exceed ~22 TW (Q_{ad}) for a dynamo in the absence of precipitation at the CMB but only ~16 TW with precipitation at the CMB occurring at our nominal rate.

Ultimately, the scaling laws for Q_{ad}, Q_{noIC}, and Q_{yesIC} have the same power-law exponent (~0.8–0.9) regardless of uncertain values for properties such as thermal conductivity. Figure S5 shows that our power laws are well-matched to our calculated values. Critically, we now know the power-law exponents with more precision than our constraints on the actual values for Earth and Venus, given uncertainties about the thermal conductivity and composition of their metallic cores. This result means that we can potentially isolate the effects of planetary mass on the prospects for a dynamo—even if many other factors remain mysterious that are potentially important to the magnetic histories of real planets.

3.2 Scaling laws for the heat flow across the core/mantle boundary

We constructed a scaling relation to describe how the cooling rate of the core changes with planetary mass. Equation 14 defines the heat flow across the CMB in terms of the properties of the boundary layer at the base of the solid mantle (Figure 2). We assume the eight mass-dependent terms in that equation obey a power laws of the form $X(M_P)/X(M_E) = (M_P/M_E)^x$, where x is a power-law exponent, analogous to Equation 15. We combine all eight power-law exponents to calculate the final scaling relation:

$$Q_{CMB}(M_P) = Q_{CMB}(M_E)\left(\frac{M_P}{M_E}\right)^{2a+b+\frac{1}{3}(c+d+e)-\frac{1}{3}(f+g)+\frac{4}{3}(h)}. \tag{16}$$

Table 4 shows that letters a, b, c, d, e, f, g, and h correspond to R_C, k_M, ρ_M, g_C, α_M, κ_M, μ_{BL}, and ΔT_{BL}, respectively. Power-law exponents for a and d, respectively associated with variables R_C and g, were derived from the values in Table 2. We report the best-fit value for each x and the formal uncertainty ("1-sigma") of the fit. Of course, the formal uncertainty is much smaller than the true uncertainty because the statistical fits are built on a series of assumptions. Table S1 lists our estimated values of these parameters at $M_P = 1$–$10M_E$. Figure S6 compares these values to their best-fit scaling laws, which provide an adequate match to the estimated values of Q_{CMB} and all of its underlying parameters except perhaps μ_{BL}.

Here is how we derived the rest of the scaling relationships:

- Thermal conductivity of the lower mantle (k_M). The thermal conductivity of silicates, which includes contributions from radiative, electronic, and phonon terms, tends to increase with temperature. Figure 9b from Stamenković et al. (2011) shows thermal conductivity as a function of pressure up to >1 TPa, assuming an adiabatic increase in temperature with pressure. We extracted values at the pressure of the CMB (P_C) for each planet (1–8 M_E) represented by that plot.
- Density of the lower mantle (ρ_M). We calculated the density of $(Mg,Fe)SiO_3$ silicate at P_C using the polytropic equation of state from Seager et al. (2007) in their Table 3. Thermal effects that are not included in that equation may change silicate densities by a few percent, which is much smaller than the variations between differently sized planets.
- Thermal expansivity of the lower mantle (α_M). Following Boujibar et al. 2020, we assumed that $\alpha_M \propto (\rho_M)^{-3}$ and thus $e = -3c$. This scaling relationship does not depend on the actual value of α_M in Earth's mantle.

- Thermal diffusivity of the lower mantle (κ_M). We assume that the lower mantles of super-Earths are hot enough that their specific heats are near the Dulong-Petit limit and thus independent of planetary mass. In this case, $\kappa_M \propto k_M/\rho_M$ by definition and $f = b - c$.
- Thermal contrast across the lower mantle boundary layer (ΔT_{BL}). By definition, $\Delta T_{BL} = T_C - T_{LM}$. We calculate T_{LM} using Equation 7 in Unterborn & Panero (2019), which is the adiabatic temperature in the lower mantle assuming a potential temperature of 1600 K for the mantle. We set T_C equal to $T_C(0)$, meaning that our scaling law applies best to planets that are on the cusp of nucleating an inner core. Noack & Lasbleis (2020) inferred similar values of ΔT_{BL} for 1- and 2-M_E planets, and also considered the effects of non-Earth-like iron contents in both the mantle and core.
- Average viscosity in the lower mantle boundary layer (μ_{BL}). Following Section 5 in Valencia & O'Connell (2009), we assume that viscosity at a given pressure decreases with temperature according to an Arrhenius law. Specifically, we assume $\mu_{BL} \propto \exp[-20(1 - T_{BL}/T_{melt})]$, where $T_{BL} = T_C - 0.5\Delta T_{BL}$ and T_{melt} is the melting temperature of $MgSiO_3$ silicates at the pressure of the CMB (Stixrude, 2014). All relevant temperatures increase rapidly with planetary mass. However, the ratio T_{BL}/T_{melt} decreases from ~0.67 to 0.60 as mass increases from ~1–10M_E. The key point is that our formulation of viscosity implies that the temperature-dependence of viscosity is slightly more important than its pressure-dependence. Even at extreme pressures, viscosities could be similar to or less than those in the lower mantle of Earth (Karato, 2011). On the other hand, significant pressure-dependence could increase the viscosity by several orders of magnitude (e.g., Noack & Lasbleis, 2020; Stamenković et al., 2012). The true uncertainty on mantle viscosity is much larger than the formal error reported in Table 4.

Overall, we estimate that $Q_{CMB}(M_P)/Q_{CMB}(M_E) = (M_P/M_E)^{1.56\pm0.06}$ or, equivalently, that $\Sigma = 1.56 \pm 0.06$, which implies that the actual heat flow across the CMB increases rapidly in comparison to the minimum value required to sustain a dynamo in the metallic core.

Figure 4 compares the four scaling laws derived in this study for Earth- and Venus-analogue planets. In this study, the only assumed difference between the two is that Q_{CMB} is relatively higher for an Earth-analogue than for a Venus-analogue. In our Solar System, the solid mantle of Earth cools fast compared to that of Venus because plate tectonics efficiently transports internal heat to the surface. Most models predict that the mantle of Venus is thus hotter than Earth's mantle at present day (e.g., Driscoll & Bercovici, 2013; Driscoll & Bercovici, 2014; O'Rourke et al., 2018). According to Eq. 14, increasing T_{LM} causes ΔT_{BL} and Q_{CMB} to decrease. Although the cores of Earth and Venus cool at different rates, we can use Eq. 16 to describe how the cooling rates of massive Earth- and Venus-analogues scale with planetary mass. For Earth, Q_{CMB} ~ 5–15 TW based on studies of mantle plumes and the thermal state of the basal mantle (e.g., Lay et al., 2008). The internal heat budget of Venus is essentially unconstrained (e.g., Smrekar et al., 2018).

Rows in Figure 4 present two types each of Earth- and Venus-analogues to reflect unknowns about real Earth and Venus. For example, we do not know if Q_{CMB} is super- or sub-adiabatic in Earth today. Earth-analogues 1 assumes $Q_{CMB} > Q_{ad}$ for a 1-M_E planet, while $Q_{yesIC} < Q_{CMB} < Q_{ad}$ at 1 M_E for Earth-analogue 2. Likewise, Q_{CMB} must be sub-adiabatic for Venus (unless its core is chemically stratified) but we do not know if an inner core exists. Venus-analogue 1 has $Q_{yesIC} < Q_{CMB} < Q_{noIC}$ for a 1-M_E planet, meaning that the absence of a dynamo would imply the absence of an inner core. Venus-analogue 2 has $Q_{CMB} < Q_{yesIC}$ at 1 M_E so even inner core growth could not sustain a dynamo. Columns in Figure 4 represent the lower (40 W/m/K) and upper (100 W/m/K) limits for the thermal conductivity of the core. Raising k_C shifts the curves representing Q_{ad}, Q_{noIC}, and Q_{yesIC} proportionally upwards. We pinned the scaling laws to higher Q_{CMB} values at 1 M_E for plots in the right column to represent the same scenarios as in the left column (i.e., super- versus sub-adiabatic Q_{CMB} for Earth and the forbidden versus permitted existence of an inner core for Venus).

According to these calculations, all planets grow increasingly likely to host a dynamo in their metallic cores as planetary mass increases. Because the power-law exponent for Q_{CMB} (~1.6) is almost twice as large as the power-law exponents for Q_{ad}, Q_{noIC}, and Q_{yesIC} (~0.8–0.9), meeting the energetic requirements for convection is more achievable in massive super-Earths and super-Venuses. Earth-analogues 1a and 1b may sustain a dynamo with thermal convection at any planetary mass. Earth-analogues 2a and 2b transition from chemical to thermochemical convection where $M_P > 1.5$ M_E. Likewise, Venus-analogues 1a and 1b are predicted to have $Q_{CMB} > Q_{ad}$ when $M_P > 1.5$ M_E (and $Q_{CMB} > Q_{noIC}$ above ~1.2 M_E). Venus-analogues 2a and 2b could host a chemically-powered dynamo above ~1.5–1.9 M_E if an inner core exists—and a thermally-powered dynamo with or without an inner core above ~4.1 (2a) or 5.8 (2b) M_E.

Overall, our nominal scalings predict that both Earth- and Venus-analogues may have strong global magnetic fields for planetary masses exceeding ~1.5 Earth-masses. Growth of an inner core is essential to driving a dynamo in massive Venus-analogues, while massive Earth-analogues have enough energy for thermal convection. At smaller terrestrial planets, the presence of a magnetosphere may signal the operation of plate tectonics (i.e., at real Earth but not real Venus). A non-detection of a magnetic field at a massive planet could be more significant than a detection. That is, massive rocky exoplanets without magnetic fields could be Venus-analogues that do not have growing inner cores, while a large rocky planet with a magnetic field could be either a super-Earth or a super-Venus. Observations of exoplanets over the next few decades will test our predictions that magnetic fields are ubiquitous for rocky planets above a certain mass. If we are correct, then magnetism may not provide a unique probe into mantle dynamics.

4 Discussion

Any study of dynamos in exoplanets must rely on simplifying assumptions and judicious speculation. Our models for the energy budgets of metallic cores are one step on a long path towards predicting the occurrence of planetary magnetism at exoplanets and, eventually, interpreting any detections. We concluded that massive planets seem relatively likely to host dynamos in their metallic cores if their silicate mantles are entirely solid. Future studies could provide straightforward extensions of our approach. For example, we only modeled planets with Earth-like core mass fractions (0.325) and Earth-like abundances of light elements (~6 wt%). Developing scaling laws for planets with Mercury-like (~0.68) and Mars-like (~0.20) core mass fractions and different amounts of impurities in the core would be an easy next step (e.g., Boujibar et al., 2020). We expect that adding light elements to the core would decrease the critical heat flow required for a dynamo in the presence of an inner core but would not change how that threshold scales with planetary mass. More importantly, the assumption that solid-state mantle convection directly governs the heat flow out of the core could be wildly inaccurate, which has big-picture implications for modeling massive exoplanets.

4.1 Towards self-consistent models of thermal evolution

Our scaling law for the heat flow across the core-mantle boundary did not fully consider how the core and mantle cool together over time. Mantle convection has been proposed to “self-regulate” so silicates at the base of the lithosphere are near their melting temperature, where mantle viscosity is minimal. However, self-regulation may not occur in relevant timescales for massive planets (Korenaga, 2016). In principle, super-Earths could have mantle potential temperatures that vary by several hundred degrees (e.g., O’Rourke & Korenaga, 2012; Stamenković et al., 2011, 2012; Tackley et al., 2013; Valencia & O’Connell, 2009). Even small differences in mantle temperatures can have dramatic effects on surface habitability—a few hundred K is the difference between catastrophic volcanism and a total dearth of volcanic and tectonic activity. However, the cores of massive super-Earths could be several thousand degrees hotter than the core of Earth because much more gravitational energy is released as heat during their formation (e.g., Boujibar et al., 2020; Noack & Lasbleis, 2020; Stixrude, 2014). The fact that T_C increases more rapidly than T_L with planetary mass is why we predict that super-Earths are relatively likely to host dynamos. However, T_C might decrease more rapidly with time relative to its initial value in super-Earths for the same reason (i.e., mantle viscosity is highly temperature-dependent). Future studies can address these issues using self-consistent models of the mantle and core.

4.2 Likelihood of a basal magma ocean

Our scaling law for the heat flow across the core-mantle boundary was built on the assumption that the silicate mantle is fully solidified. Indeed, Table S1 shows that the existence of an inner core implies temperatures at the top of the core that are below the melting point of silicates at the relevant pressures, according to one parameterization in Stixrude (2014). However, the melting temperature of silicates is highly sensitive to their composition. Boujibar et al. (2020) showed that an inner core may co-exist with a partially liquid lower mantle. If temperatures in the lower mantle are high enough, there could be a global layer of molten silicates called a basal magma ocean (BMO). Labrosse et al. (2007) proposed that Earth itself had a BMO that took a few billion years to solidify. O’Rourke (2020) speculated that a BMO may still exist within Venus today. A BMO would dramatically affect the heat and dissipation budgets for the metallic core.

Crucially, a BMO vastly reduces the cooling rate of the core because its secular cooling and latent heat subtracts from the heat budget. That is, the heat that we predicted the solid mantle would extract from the core would actually be the total amount of heat extracted from the BMO and the core. Because the BMO is a heat sink, the cooling rate of the core can be decreased by a factor of two or greater. Models generally predict that a thick BMO reduces the heat flow out of the core to levels that are sub-critical for a dynamo (e.g., Blanc et al., 2020; Labrosse et al., 2007; O'Rourke, 2020; Ziegler & Stegman, 2013). However, the BMO itself may host a dynamo because liquid silicates are electrically conductive under extreme pressures and temperatures (e.g., Holmström et al., 2018; Scipioni et al., 2017; Soubiran & Militzer, 2018; Stixrude et al., 2020). Planets could transition from a BMO-hosted to a core-hosted dynamo over time as they cool (Ziegler & Stegman, 2013). Speculatively, a BMO-hosted dynamo could produce a stronger magnetosphere because the dynamo-generating region is closer to the surface. No study has yet modeled the prospects for a dynamo in the BMO of massive exoplanets—but such studies are obviously a very high priority. Our models for the energetics of metallic cores would easily interface with more detailed descriptions of the silicate mantle with or without a BMO.

5 Conclusions

Here we presented a model for the energetics of dynamos in the metallic cores of super-Earth exoplanets. The model is built on a one-dimensional (radial) parameterization of the density and pressure within the liquid portion of the core, which is assumed to maintain an adiabatic thermal gradient due to vigorous convection. The total dissipation available for a dynamo is calculated using the energy and entropy budgets for the core. Overall, we considered four sources of thermal buoyancy and two sources of chemical buoyancy that can help drive convection. We developed a simple scaling law to roughly estimate how the actual heat flow across the core-mantle boundary (CMB) may vary with planetary mass for comparison to the critical thresholds required for a dynamo with and without an inner core.

Our main conclusions are as follows:

1. The minimum heat flows necessary to provoke thermal and chemical convection in the liquid part of the core increase with planetary mass according to power laws with exponents of ~0.8–0.9. These power-law exponents are insensitive to properties of the core such as its thermal conductivity, the rate at which light elements precipitate at the

CMB, and the amount of radiogenic heating—all of which are uncertain even for Earth and impossible to directly constrain using available techniques for exoplanets.

2. An inner core vastly increases the likelihood of a dynamo, especially within massive planets. Fortunately, the critical heat flow required for a dynamo is not very sensitive to the exact radius of the inner core. We lack direct constraints on the size of the inner core even for most rocky planetary bodies in our Solar System besides Earth.
3. The actual heat flow across the CMB is predicted to increase with planetary mass according to a power law with an exponent of ~1.6 for both Earth- and Venus-analogues. Of the eight terms that feed into this scaling law, viscosity is likely the most uncertain. We inferred that super-Earths and Earth have similar mantle viscosities, but other studies predict that silicates become very viscous at extreme pressures. That said, viscosity would have to increase by the square of planetary mass (i.e., a ~10 Earth-mass planet having ~100 times the mantle viscosity of Earth) to reduce the power-law exponent to ~0.9 to match the scaling laws for the minimum heat flow to drive a dynamo.
4. As planetary mass increases, the predicted rates of inner core growth and temperature change in the outer core both decrease rapidly. Because enormous cores are enormous heat sinks, inner cores may not nucleate for many billions of years unless core temperatures are initially near the liquidus. Thermal evolution models are required to explore these possibilities.
5. Detecting a magnetic field would not prove that a super-Earth larger than ~1.5 Earth-masses is a true Earth-analogue (i.e., with relatively rapid mantle cooling possibly attributable to plate tectonics). However, the absence of a magnetic field is still a clue that a super-Earth does not have Earth-like mantle dynamics. Venus might have an inner core but no dynamo today. Scaled-up versions of Venus could sustain chemical convection in the core even in the absence of plate tectonics if they have an inner core. Thermal convection alone might not produce a dynamo in Venus-analogues smaller than ~4 Earth-masses. In contrast, virtually every massive Earth-analogue should host a dynamo even if an inner core has not yet nucleated.

Future studies should consider non-Earth-like compositions and core mass fractions—and should self-consistently model the thermal evolution of the core and mantle. Perhaps most importantly, a basal magma ocean in the lower mantle of a super-Earth would substantially decrease the heat flow out of the core relative to the scaling law we developed assuming a solid mantle. Because silicates within the basal magma ocean would be electrically conductive, the basal magma ocean itself could sustain a dynamo even as it suppresses convection within the core.

Acknowledgments

Two anonymous reviewers and the editor provided many helpful suggestions that improved the content and clarity of our manuscript. All the data sets required to create the Figures and Tables are available in the main text, the Supporting Information, and the repository platform *Open Science Framework* (O'Rourke, 2021). In particular, Jupyter notebooks that can reproduce Figures 1 and 3 and Tables 2 and 3 are archived with the repository platform.

References

Aubert, J., Labrosse, S., & Poitou, C. (2009). Modelling the palaeo-evolution of the geodynamo. *Geophysical Journal International*, *179*(3), 1414–1428. https://doi.org/10.1111/j.1365-246X.2009.04361.x

Badro, J., Siebert, J., & Nimmo, F. (2016). An early geodynamo driven by exsolution of mantle components from Earth's core. *Nature*, *536*(7616), 326–328. https://doi.org/10.1038/nature18594

Badro, J., Aubert, J., Hirose, K., Nomura, R., Blanchard, I., Borensztajn, S., & Siebert, J. (2018). Magnesium Partitioning Between Earth's Mantle and Core and its Potential to Drive an Early Exsolution Geodynamo. *Geophysical Research Letters*, *45*(24), 13,240-13,248. https://doi.org/10.1029/2018GL080405

Bercovici, D., & Ricard, Y. (2014). Plate tectonics, damage and inheritance. *Nature*, *508*(7497), 513–6. https://doi.org/10.1038/nature13072

Blanc, N. A., Stegman, D. R., & Ziegler, L. B. (2020). Thermal and magnetic evolution of a crystallizing basal magma ocean in Earth's mantle. *Earth and Planetary Science Letters*, *534*, 116085. https://doi.org/10.1016/j.epsl.2020.116085

Blanchard, I., Siebert, J., Borensztajn, S., & Badro, J. (2017). The solubility of heat-producing elements in Earth's core. *Geochemical Perspectives Letters*, 1–5. https://doi.org/10.7185/geochemlet.1737

Bonati, I., Lasbleis, M., & Noack, L. (2020). Structure and thermal evolution of exoplanetary cores. *Earth and Space Science Open Archive*. https://doi.org/10.1002/essoar.10504524.1

Bono, R. K., Tarduno, J. A., Nimmo, F., & Cottrell, R. D. (2019). Young inner core inferred from Ediacaran ultra-low geomagnetic field intensity. *Nature Geoscience*, *12*(2), 143–147. https://doi.org/10.1038/s41561-018-0288-0

Boujibar, A., Driscoll, P., & Fei, Y. (2020). Super-Earth Internal Structures and Initial Thermal States. *Journal of Geophysical Research: Planets*, *125*(5), e2019JE006124. https://doi.org/10.1029/2019JE006124

Buffett, B. A., Garnero, E. J., & Jenaloz, R. (2000). Sediments at the Top of Earth's Core. *Science*, *290*(5495), 1338–1342. https://doi.org/10.1126/science.290.5495.1338

Chidester, B. A., Rahman, Z., Righter, K., & Campbell, A. J. (2017). Metal-silicate partitioning of U: Implications for the heat budget of the core and evidence for reduced U in the mantle. *Geochimica et Cosmochimica Acta*, *199*, 1–12. https://doi.org/10.1016/j.gca.2016.11.035

Christensen, U. R. (2010). Dynamo Scaling Laws and Applications to the Planets. *Space Science Reviews*, *152*(1–4), 565–590. https://doi.org/10.1007/s11214-009-9553-2

Dong, C., Jin, M., & Lingam, M. (2020). Atmospheric Escape From TOI-700 d: Venus versus Earth Analogs. *The Astrophysical Journal*, *896*(2), L24. https://doi.org/10.3847/2041-8213/ab982f

Driscoll, P., & Bercovici, D. (2013). Divergent evolution of Earth and Venus: Influence of degassing, tectonics, and magnetic fields. *Icarus*, *226*(2), 1447–1464. https://doi.org/10.1016/j.icarus.2013.07.025

Driscoll, P. E. (2018). Planetary Interiors, Magnetic Fields, and Habitability. In H. J. Deeg & J. A. Belmonte (Eds.), *Handbook of Exoplanets* (pp. 1–18). Springer International Publishing. https://doi.org/10.1007/978-3-319-30648-3_76-1

Driscoll, P, & Bercovici, D. (2014). On the thermal and magnetic histories of Earth and Venus: Influences of melting, radioactivity, and conductivity. *Physics of the Earth and Planetary Interiors*, *236*, 36–51. https://doi.org/10.1016/j.pepi.2014.08.004

Driscoll, Peter, & Olson, P. (2011). Optimal dynamos in the cores of terrestrial exoplanets: Magnetic field generation and detectability. *Icarus*, *213*(1), 12–23. https://doi.org/10.1016/j.icarus.2011.02.010

Du, Z., Boujibar, A., Driscoll, P., & Fei, Y. (2019). Experimental Constraints on an MgO Exsolution-Driven Geodynamo. *Geophysical Research Letters*, *46*(13), 7379–7385. https://doi.org/10.1029/2019GL083017

Dumoulin, C., Tobie, G., Verhoeven, O., Rosenblatt, P., & Rambaux, N. (2017). Tidal constraints on the interior of Venus. *Journal of Geophysical Research: Planets*, *122*(6), 1338–1352. https://doi.org/10.1002/2016JE005249

Foley, B. J., & Driscoll, P. E. (2016). Whole planet coupling between climate, mantle, and core: Implications for rocky planet evolution. *Geochemistry, Geophysics, Geosystems*, *17*(5), 1885–1914. https://doi.org/10.1002/2015GC006210

Foley, B. J., Bercovici, D., & Landuyt, W. (2012). The conditions for plate tectonics on super-Earths: Inferences from convection models with damage. *Earth and Planetary Science Letters*, *331–332*, 281–290. https://doi.org/10.1016/j.epsl.2012.03.028

Gaidos, E., Conrad, C. P., Manga, M., & Hernlund, J. (2010). Thermodynamic limits on magnetodynamos in rocky exoplanets. *Astrophysical Journal*, *718*(2), 596–609. https://doi.org/10.1088/0004-637X/718/2/596

Hirose, K., Labrosse, S., & Hernlund, J. (2013). Composition and State of the Core. *Annual Review of Earth and Planetary Sciences*, *41*(1), 657–691. https://doi.org/10.1146/annurev-earth-050212-124007

Hirose, K., Morard, G., Sinmyo, R., Umemoto, K., Hernlund, J., Helffrich, G., & Labrosse, S. (2017). Crystallization of silicon dioxide and compositional evolution of the Earth's core. *Nature*, *543*(7643), 99–102. https://doi.org/10.1038/nature21367

Holmström, E., Stixrude, L., Scipioni, R., & Foster, A. S. (2018). Electronic conductivity of solid and liquid (Mg, Fe)O computed from first principles. *Earth and Planetary Science Letters*, *490*, 11–19. https://doi.org/10.1016/j.epsl.2018.03.009

Jacobson, S. A., Rubie, D. C., Hernlund, J., Morbidelli, A., & Nakajima, M. (2017). Formation, stratification, and mixing of the cores of Earth and Venus. *Earth and Planetary Science Letters*, *474*, 375–386. https://doi.org/10.1016/j.epsl.2017.06.023

Kane, S. R., Barclay, T., & Gelino, D. M. (2013). A POTENTIAL SUPER-VENUS IN THE KEPLER-69 SYSTEM. *The Astrophysical Journal*, *770*(2), L20. https://doi.org/10.1088/2041-8205/770/2/L20

Kane, S. R., Kopparapu, R. K., & Domagal-Goldman, S. D. (2014). On the frequency of potential Venus analogs from Kepler data. *Astrophysical Journal Letters*, *794*(1).

https://doi.org/10.1088/2041-8205/794/1/L5

Kane, S. R., Arney, G., Crisp, D., Domagal-Goldman, S., Glaze, L. S., Goldblatt, C., et al. (2019). Venus as a Laboratory for Exoplanetary Science. *Journal of Geophysical Research: Planets*, *124*(8), 2015–2028. https://doi.org/10.1029/2019JE005939

Karato, S. (2011). Rheological structure of the mantle of a super-Earth: Some insights from mineral physics. *Icarus*, *212*(1), 14–23. https://doi.org/10.1016/j.icarus.2010.12.005

Korenaga, J. (2012). Plate tectonics and planetary habitability: current status and future challenges. *Annals of the New York Academy of Sciences*, *1260*, 87–94. https://doi.org/10.1111/j.1749-6632.2011.06276.x

Korenaga, J. (2016). Can mantle convection be self-regulated? *Science Advances*, *2*(8), e1601168. https://doi.org/10.1126/sciadv.1601168

Labrosse, S. (2015). Thermal evolution of the core with a high thermal conductivity. *Physics of the Earth and Planetary Interiors*, *247*, 36–55. https://doi.org/dx

Labrosse, S., Hernlund, J. W., & Coltice, N. (2007). A crystallizing dense magma ocean at the base of the Earth's mantle. *Nature*, *450*(7171), 866–9. https://doi.org/10.1038/nature06355

Landeau, M., Aubert, J., & Olson, P. (2017). The signature of inner-core nucleation on the geodynamo. *Earth and Planetary Science Letters*, *465*, 193–204. https://doi.org/10.1016/j.epsl.2017.02.004

Lay, T., Hernlund, J., & Buffett, B. A. (2008). Core–mantle boundary heat flow. *Nature Geoscience*, *1*(1), 25–32. https://doi.org/10.1038/ngeo.2007.44

Liu, W., Zhang, Y., Yin, Q.-Z., Zhao, Y., & Zhang, Z. (2019). Magnesium partitioning between silicate melt and liquid iron using first-principles molecular dynamics: Implications for the early thermal history of the Earth's core. *Earth and Planetary Science Letters*, *1*, 115934. https://doi.org/10.1016/J.EPSL.2019.115934

Mittal, T., Knezek, N., Arveson, S. M., McGuire, C. P., Williams, C. D., Jones, T. D., & Li, J. (2020). Precipitation of multiple light elements to power Earth's early dynamo. *Earth and Planetary Science Letters*, *532*, 116030. https://doi.org/10.1016/j.epsl.2019.116030

Nimmo, F. (2002). Why does Venus lack a magnetic field? *Geology*, *30*(11), 987–990. https://doi.org/10.1130/0091-7613(2002)030<0987:WDVLAM>2.0.CO;2

Nimmo, F. (2015a). Energetics of the Core. In *Treatise on Geochemistry: Second Edition* (Vol. 1, pp. 31–65). Elsevier B.V. https://doi.org/10.1016/B978-044452748-6.00128-0

Nimmo, F. (2015b). Thermal and Compositional Evolution of the Core. In *Treatise on Geochemistry: Second Edition* (Vol. 9, pp. 217–241). Elsevier B.V. https://doi.org/10.1016/B978-044452748-6.00147-4

Noack, L., & Lasbleis, M. (2020). Parameterisations of interior properties of rocky planets: An investigation of planets with Earth-like compositions but variable iron content. *Astronomy and Astrophysics*, *638*. https://doi.org/10.1051/0004-6361/202037723

O'Rourke, J. G. (2020). Venus: A Thick Basal Magma Ocean May Exist Today. *Geophysical Research Letters*, *47*(4). https://doi.org/10.1029/2019GL086126

O'Rourke, J. G. (2021). Energetic Requirements for Dynamos in the Metallic Cores of Super-

Earth and Super-Venus Exoplanets. Open Science Framework. https://doi.org/10.17605/OSF.IO/XG8C2

O'Rourke, J. G., & Korenaga, J. (2012). Terrestrial planet evolution in the stagnant-lid regime: Size effects and the formation of self-destabilizing crust. *Icarus*, *221*(2), 1043–1060. https://doi.org/10.1016/j.icarus.2012.10.015

O'Rourke, J. G., & Stevenson, D. J. (2016). Powering Earth's dynamo with magnesium precipitation from the core. *Nature*, *529*(7586), 387–389. https://doi.org/10.1038/nature16495

O'Rourke, J. G., Gillmann, C., & Tackley, P. (2018). Prospects for an ancient dynamo and modern crustal remanent magnetism on Venus. *Earth and Planetary Science Letters*, *502*, 46–56. https://doi.org/10.1016/j.epsl.2018.08.055

Pozzo, M., Davies, C., Gubbins, D., & Alfè, D. (2012). Thermal and electrical conductivity of iron at Earth's core conditions. *Nature*, *485*(7398), 355–8. https://doi.org/10.1038/nature11031

Rogers, L. A. (2015). Most 1.6 earth-radius planets are not rocky. *Astrophysical Journal*, *801*(1), 41. https://doi.org/10.1088/0004-637X/801/1/41

Scipioni, R., Stixrude, L., & Desjarlais, M. P. (2017). Electrical conductivity of SiO2 at extreme conditions and planetary dynamos. *Proceedings of the National Academy of Sciences of the United States of America*, *114*(34), 9009–9013. https://doi.org/10.1073/pnas.1704762114

Seager, S., Kuchner, M., Hier-Majumder, C. A., & Militzer, B. (2007). Mass-Radius Relationships for Solid Exoplanets. *ApJ*, *669*(2), 1279–1297. https://doi.org/10.1086/521346

Seagle, C. T., Cottrell, E., Fei, Y., Hummer, D. R., & Prakapenka, V. B. (2013). Electrical and thermal transport properties of iron and iron-silicon alloy at high pressure. *Geophysical Research Letters*, *40*(20), 5377–5381. https://doi.org/10.1002/2013GL057930

Smrekar, S. E., Davaille, A., & Sotin, C. (2018). Venus Interior Structure and Dynamics. *Space Science Reviews*, *214*(5), 88. https://doi.org/10.1007/s11214-018-0518-1

Sotin, C., Grasset, O., & Mocquet, A. (2007). Mass-radius curve for extrasolar Earth-like planets and ocean planets. *Icarus*, *191*(1), 337–351. https://doi.org/10.1016/j.icarus.2007.04.006

Soubiran, F., & Militzer, B. (2018). Electrical conductivity and magnetic dynamos in magma oceans of Super-Earths. *Nature Communications*, *9*(1). https://doi.org/10.1038/s41467-018-06432-6

Stamenković, V., Breuer, D., & Spohn, T. (2011). Thermal and transport properties of mantle rock at high pressure: Applications to super-Earths. *Icarus*, *216*(2), 572–596. https://doi.org/10.1016/j.icarus.2011.09.030

Stamenković, V., Noack, L., Breuer, D., & Spohn, T. (2012). the Influence of Pressure-Dependent Viscosity on the Thermal Evolution of Super-Earths. *ApJ*, *748*(1), 41. https://doi.org/10.1088/0004-637X/748/1/41

Stelzer, Z., & Jackson, A. (2013). Extracting scaling laws from numerical dynamo models. *Geophysical Journal International*, *193*(3), 1265–1276. https://doi.org/10.1093/gji/ggt083

Stevenson, D. J. (2003). Planetary magnetic fields. *Earth and Planetary Science Letters*, *208*(1–2), 1–11. https://doi.org/10.1016/S0012-821X(02)01126-3

Stevenson, D. J. (2010). Planetary magnetic fields: Achievements and prospects. *Space Science Reviews*, *152*(1–4), 651–664. https://doi.org/10.1007/s11214-009-9572-z

Stevenson, D. J., Spohn, T., & Schubert, G. (1983). Magnetism and thermal evolution of the terrestrial planets. *Icarus*, *54*(3), 466–489. https://doi.org/10.1016/0019-1035(83)90241-5

Stixrude, L. (2014). Melting in super-earths. *Philosophical Transactions of the Royal Society A: Mathematical, Physical and Engineering Sciences*, *372*(2014), 20130076. https://doi.org/10.1098/rsta.2013.0076

Stixrude, L., Scipioni, R., & Desjarlais, M. P. (2020). A silicate dynamo in the early Earth. *Nature Communications*, *11*(1), 935. https://doi.org/10.1038/s41467-020-14773-4

Van Summeren, J., Gaidos, E., & Conrad, C. P. (2013). Magnetodynamo lifetimes for rocky, Earth-mass exoplanets with contrasting mantle convection regimes. *Journal of Geophysical Research E: Planets*, *118*(5), 938–951. https://doi.org/10.1002/jgre.20077

Tachinami, C., Senshu, H., & Ida, S. (2011). Thermal evolution and lifetime of intrinsic magnetic fields of super-earths in habitable zones. *Astrophysical Journal*, *726*(2). https://doi.org/10.1088/0004-637X/726/2/70

Tackley, P. J., Ammann, M., Brodholt, J. P., Dobson, D. P., & Valencia, D. (2013). Mantle dynamics in super-Earths: Post-perovskite rheology and self-regulation of viscosity. *Icarus*, *225*(1), 50–61. https://doi.org/10.1016/j.icarus.2013.03.013

Tasker, E., Tan, J., Heng, K., Kane, S., Spiegel, D., Brasser, R., et al. (2017). The language of exoplanet ranking metrics needs to change. *Nature Astronomy*, *1*(February), 1–2. https://doi.org/10.1038/s41550-017-0042

Unterborn, C. T., & Panero, W. R. (2019). The Pressure and Temperature Limits of Likely Rocky Exoplanets. *Journal of Geophysical Research: Planets*, *124*, 1704–1716. https://doi.org/10.1029/2018JE005844

Valencia, D., & O'Connell, R. J. (2009). Convection scaling and subduction on Earth and super-Earths. *Earth and Planetary Science Letters*, *286*(3–4), 492–502. https://doi.org/10.1016/j.epsl.2009.07.015

Valencia, D., O'Connell, R. J., & Sasselov, D. (2006). Internal structure of massive terrestrial planets. *Icarus*, *181*(2), 545–554. https://doi.org/10.1016/j.icarus.2005.11.021

Weiss, L. M., & Marcy, G. W. (2014). The mass-radius relation for 65 exoplanets smaller than 4 earth radii. *Astrophysical Journal Letters*, *783*(1), 1–7. https://doi.org/10.1088/2041-8205/783/1/L6

Wicks, J. K., Smith, R. F., Fratanduono, D. E., Coppari, F., Kraus, R. G., Newman, M. G., et al. (2018). Crystal structure and equation of state of Fe-Si alloys at super-Earth core conditions. *Science Advances*, *4*(4). https://doi.org/10.1126/sciadv.aao5864

Zhang, Y., Hou, M., Driscoll, P., Salke, N. P., Liu, J., Greenberg, E., et al. (2021). Transport properties of Fe-Ni-Si alloys at Earth's core conditions: Insight into the viability of thermal and compositional convection. *Earth and Planetary Science Letters*, *553*, 116614.

https://doi.org/10.1016/j.epsl.2020.116614

Ziegler, L. B., & Stegman, D. R. (2013). Implications of a long-lived basal magma ocean in generating Earth's ancient magnetic field. *Geochemistry, Geophysics, Geosystems*, *14*(11), 4735–4742. https://doi.org/10.1002/2013GC005001

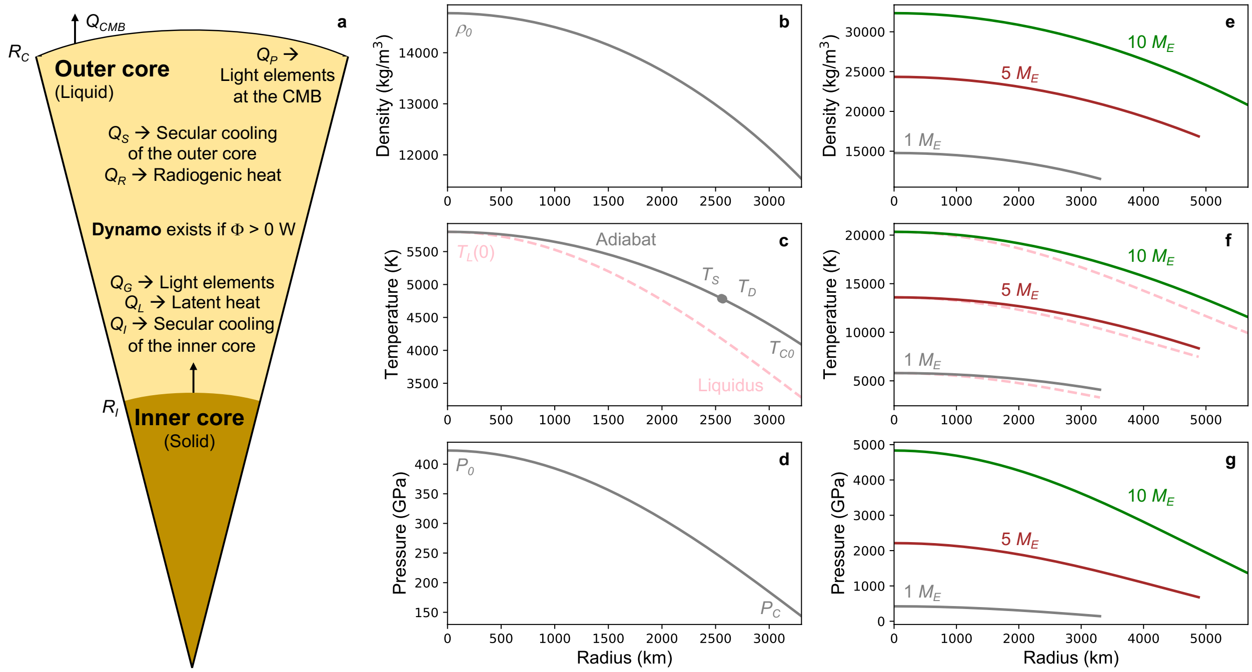

Figure 1. Internal structure of the core. We obtain analytic equations for density, temperature, and pressure as a function of radius. To start, the core is entirely liquid and chemically homogenous. (a) As it cools, an inner core begins to freeze from the center outwards. The total heat flow across the core-mantle boundary (Q_{CMB}) is partitioned between six different energy terms in the outer core (Q_P, Q_R, Q_S, Q_G, Q_I, and Q_L). Grey lines in the middle panels show the radial profiles of (b) density, (c) temperature, and (d) pressure in a 1 Earth-mass (M_E) planet. Here the temperature at the core-mantle boundary (T_{C0}) is chosen so the inner core is on the cusp of nucleating. The adiabat (grey line) intersects the liquidus (pink, dashed line) at the center of the core, i.e., at temperature $T_L(0)$. The right-hand panels show the radial profiles of (e) density, (f) temperature, and (g) pressure for 1 M_E (grey), 5 M_E (brown), and 10 M_E (green) planets. These internal structures are nearly identical to those in Boujibar et al. (2020) except we neglected thermal effects and did not model the mantle.

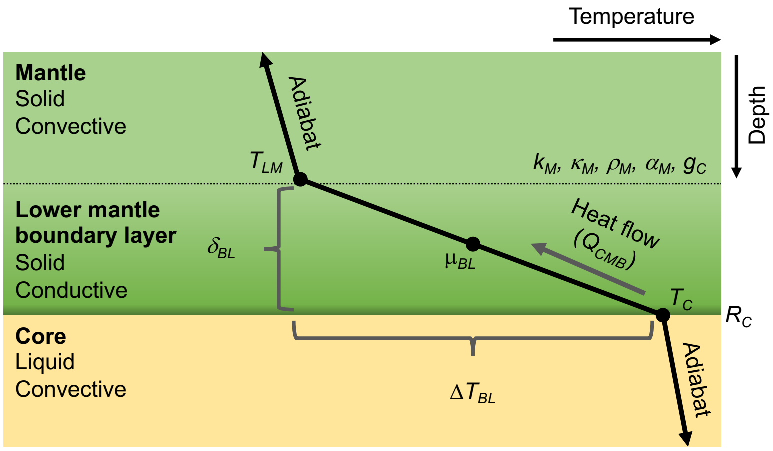

Figure 2. Cartoon of the boundary layer at the base of the solid mantle. We use this model to estimate how the heat flow across the core-mantle boundary (Q_{CMB}) scales with planetary mass. Listed variables are defined in the main text. A thermal boundary layer exists also at the top of the core. However, the core-side boundary layer is several orders of magnitude thinner than the boundary layer in the lower mantle because the solid mantle is >20 orders of magnitude more viscous than the liquid core.

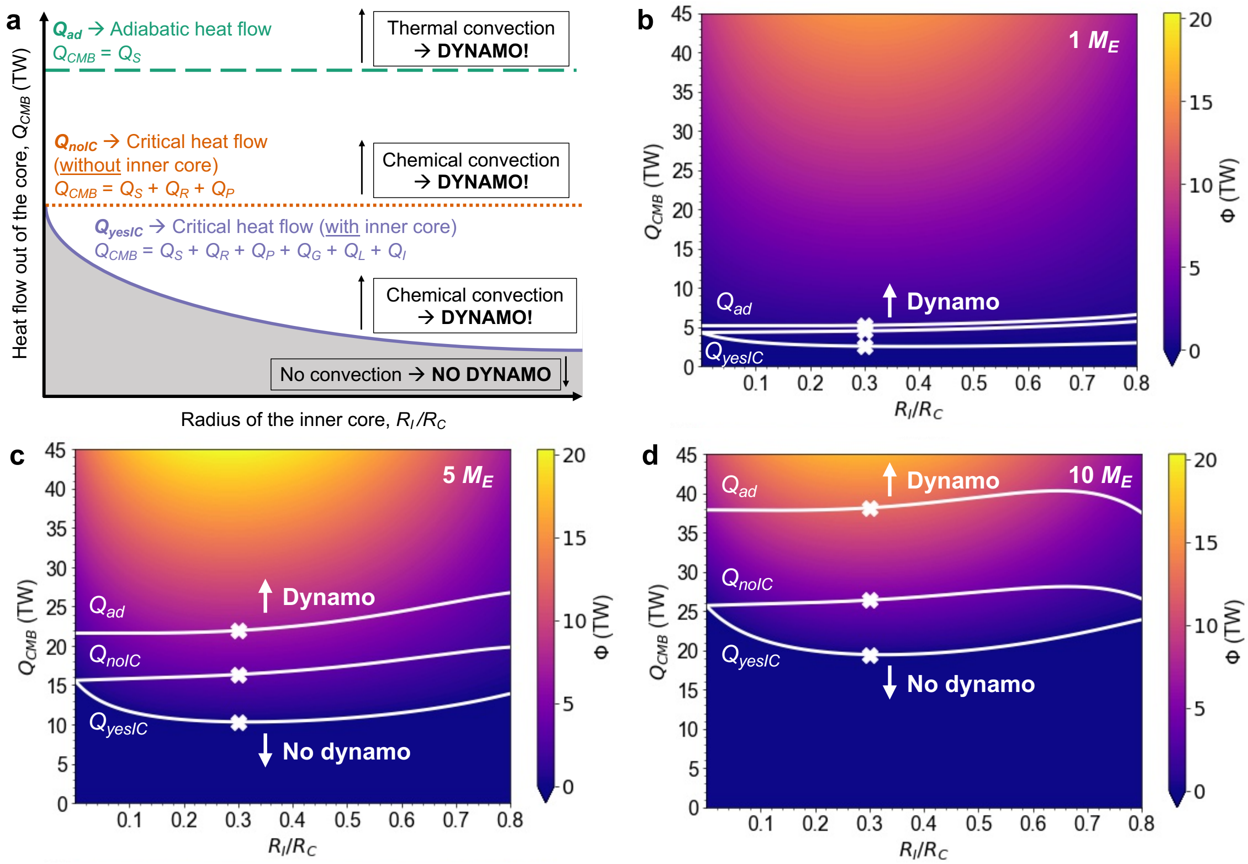

Figure 3. Energetic requirements for dynamos in the cores of massive rocky planets are not very sensitive to the radius of the inner core. We assume that super-Earth and super-Venus cores have the same structures and compositions, so these diagrams apply to both types of exoplanets. (a) Cartoon regime diagram showing the three threshold heat flows: the adiabatic heat flow (Q_{ad}) and the critical values in the absence (Q_{noIC}) and presence (Q_{yesIC}) of an inner core. We varied two parameters: Q_{CMB}, the heat flow across the core-mantle boundary, and R_I/R_C, the normalized inner core radius. We calculated the total dissipation (color shading) available to drive a dynamo for 1 M_E (b), 5 M_E (c), 10 M_E (d) exoplanets assuming $k_C = 40$ W/m/K, [K] = 50 ppm, and $P_P = 5 \times 10^{-6}$ K^{-1}. Crosses on Q_{yesIC}, Q_{noIC}, and Q_{ad} (white lines) in (b), (c), and (d) show representative values that were extracted for Table 3.

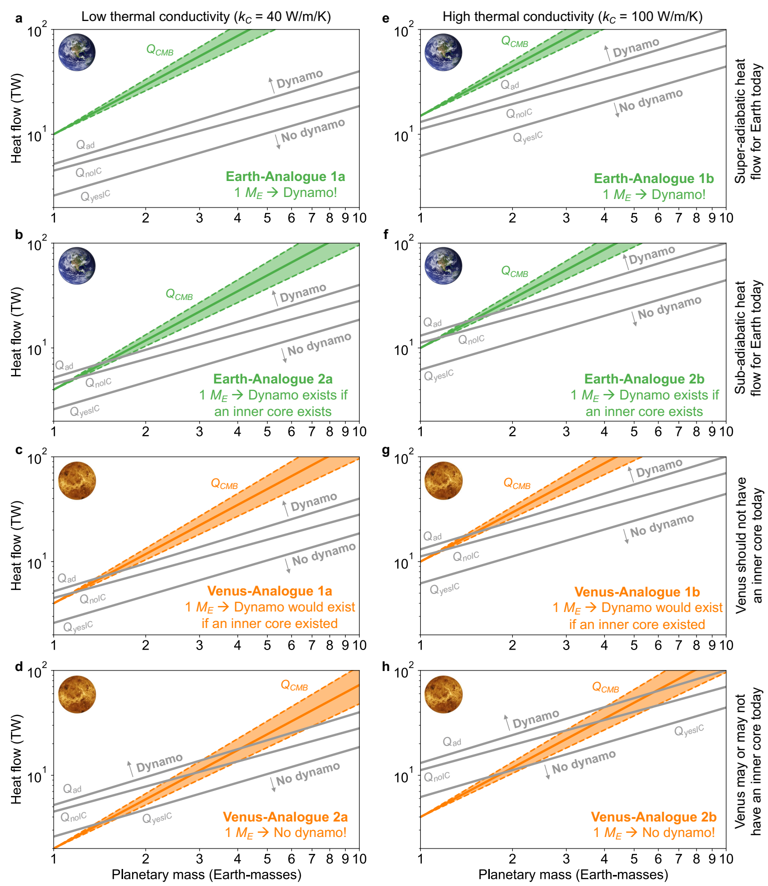

Figure 4. The likelihood of a dynamo in the metallic cores of rocky exoplanets may increase with planetary mass if their lower mantles are completely solid. Each subplot shows how the actual heat flow across the core-mantle boundary (Q_{CMB}) and the minimum values required to drive thermal convection (Q_{ad}) and chemical convection in the absence (Q_{noIC}) or presence (Q_{yesIC}) of an inner core scale with planetary mass. Solid lines show the nominal scaling for Q_{CMB}, and the shaded region bordered by dashed lines indicates three times the formal uncertainty (3-σ) from Table 3. The power-law fits for Q_{ad}, Q_{noIC}, and Q_{yesIC} have negligible formal uncertainties. Plots in the left and right columns were generated assuming lower and upper limits of 40 and 100 W/m/K, respectively, for the thermal conductivity of the outer core. We pinned the scaling law for Q_{CMB} to different values at 1 M_E to represent different scenarios for the current state of Earth and Venus. Panels (a) and (e) represent Earth-analogues with super-adiabatic heat flow across the CMB. Panels (b) and (f) show Earth-analogues with sub-adiabatic heat flow at 1 M_E. Panels (c) and (g) illustrate the scaling laws for Venus-analogues that would always have a dynamo if an inner core exists. Finally, panels (d) and (h) demonstrate that even Venus-analogues with $Q_{CMB} < Q_{yesIC}$ at 1 M_E might have dynamos at higher planetary masses.

Table 1
Definitions of Key Model Inputs and Outputs

Variable	Definition	Units
Structure and composition of the core		
t	Time	Gyr
k_C	Thermal conductivity of the core	W/m/K
P_P	Precipitation rate of light elements at the core-mantle boundary	1/K
[K]	Abundance of potassium in the core	ppm
R_I	Radius of the inner core	km
$T_L(R_I)$	Liquidus temperature at the inner core boundary	K
T_D	Average temperature in the outer core	K
T_S	Temperature associated with specific heat in the outer core	K
T_C	Temperature at the core-mantle boundary	K
Heat budget for the outer core		
Q_{CMB}	Total heat flow across the core-mantle boundary	TW
Q_S	Secular cooling of the outer core	TW
Q_R	Radiogenic heat in the core	TW
Q_P	Gravitational heat from precipitation of light elements at the core-mantle boundary	TW
Q_G	Gravitational heat from exclusion of light elements from the inner core	TW
Q_L	Latent heat from the growth of the inner core	TW
Q_I	Secular cooling of the inner core	TW
Dissipation budget for the outer core (n.b., a dynamo exists if $\Phi > 0$ TW)		
Φ	Total dissipation available for a dynamo	TW
Φ_S	Dissipation associated with secular cooling of the outer core	TW
Φ_R	Dissipation associated with radiogenic heat	TW
Φ_P	Dissipation associated with the precipitation of light elements	TW
Φ_G	Dissipation associated with light elements from the inner core	TW
Φ_L	Dissipation associated with latent heat of the inner core	TW
Φ_I	Dissipation associated with secular cooling of the inner core	TW
Φ_K	Dissipation sink associated with thermal conduction in the outer core	TW
Q_{ad}	Adiabatic heat flow in the core	TW
Q_{noIC}	Minimum value of Q_{CMB} required to drive a dynamo in the absence of an inner core but including radiogenic heat and the precipitation of light elements	TW
Q_{yesIC}	Minimum value of Q_{CMB} required to drive a dynamo by thermochemical convection with an inner core and all other available power sources	TW

852

Table 2
Structural parameters for the metallic cores of super-Earths were computed following Boujibar et al. (2020) and Labrosse (2015).

			Planetary Mass (M_P) in Units of Earth-Masses (M_E)									
Term	**Units**	**Description**	**1**	**2**	**3**	**4**	**5**	**6**	**7**	**8**	**9**	**10**
M_C	10^{24} kg	Total mass of the core	1.94	3.88	5.82	7.76	9.70	11.6	13.6	15.5	17.5	19.4
R_P	km	Radius of the planet	6371	7682	8571	9263	9839	10335	10774	11170	11531	11863
R_C	km	Radius of the core	3301	3940	4343	4643	4884	5086	5261	5413	5551	5675
ρ_0	kg/m^3	Density at the center of the core	14775	17837	20290	22419	24339	26117	27787	29364	30879	32341
K_0	GPa	Effective bulk modulus	1657	2881	4097	5310	6529	7757	8995	10234	11490	12758
K_1		Derivative of the effective bulk modulus	3.548	3.162	2.948	2.806	2.703	2.620	2.559	2.505	2.460	2.421
L_ρ	km	Length scale in the density profile	7372	8051	8438	8696	8881	9021	9130	9216	9285	9342
A_ρ		Constant in the density profile	0.474	0.281	0.174	0.103	0.0516	0.0116	-0.0206	-0.0474	-0.0701	-0.0897
$P(0)$	GPa	Pressure at the center of the core	423	834	1273	1733	2212	2707	3219	3742	4282	4834
P_C	GPa	Pressure at the core/mantle boundary	144	273	408	546	683	822	959	1097	1234	1370
γ		Grüneisen parameter (mass-weighted average)	1.41	1.38	1.36	1.34	1.33	1.32	1.31	1.30	1.29	1.28
$T_L(0)$	K	Liquidus temperature at the center of the core	5800	8227	10229	11991	13596	15087	16494	17824	19106	20337
$T_C(0)$	K	CMB temperature when the inner core nucleates	4089	5474	6579	7528	8346	9085	9765	10399	10994	11560
dT_L/dP	K/GPa	Change in liquidus temperature with pressure	9	7	5	5	4	4	4	3	3	3
g_C	m/s^2	Gravitational acceleration at the core/mantle boundary	11.9	16.7	20.6	24.0	27.1	29.9	32.7	35.3	37.9	40.2
α_T	10^{-5}/K	Coefficient of thermal expansion (mass-weighted average)	2.7	2.5	2.4	2.3	2.2	2.2	2.1	2.1	2.0	2.0

853

Table 3

We calculated the minimum heat flow required to sustain convection and thus a dynamo before the inner core nucleates (Q_{noIC}), after the inner core nucleates (Q_{yesIC}), and the adiabatic heat flow that would be required in the absence of radiogenic heating and/or chemical buoyancy (Q_{ad}). Different combinations of [K], P_P, and k_C were chosen to study the effects of these three parameters. Plots of the energetic regime diagrams similar to Figure 3 for all parameter choices and planetary masses are included in the Supporting Information and can be reproduced using the software available in a repository (O'Rourke, 2021). We fit power laws to the results for each set of parameters to determine how the requirements for a dynamo scale with planetary mass.

	Nominal values. [K] = 50 ppm, $P_P = 5 \times 10^{-6}$ K^{-1}, k_C = 40 W/m/K			Radiogenic heating. [K] = 200 ppm, $P_P = 5 \times 10^{-6}$ K^{-1}, k_C = 40 W/m/K			Thermal conductivity. [K] = 50 ppm, $P_P = 5 \times 10^{-6}$ K^{-1}, k_C = 100 W/m/K			Precipitation at the CMB. [K] = 50 ppm, $P_P = 0$ K^{-1}, k_C = 40 W/m/K		
M_P (M_E)	Q_{ad} (TW)	Q_{noIC} (TW)	Q_{yesIC} (TW)	Q_{ad} (TW)	Q_{noIC} (TW)	Q_{yesIC} (TW)	Q_{ad} (TW)	Q_{noIC} (TW)	Q_{yesIC} (TW)	Q_{ad} (TW)	Q_{noIC} (TW)	Q_{yesIC} (TW)
1	5.2	4.5	2.6	5.2	4.7	3.1	13.1	11.2	6.2	5.2	5.2	2.7
2	9.7	7.9	4.8	9.6	8.3	5.9	24.1	19.4	11.4	9.6	9.7	5.0
3	13.8	10.9	6.4	13.8	11.7	8.2	34.5	26.9	15.1	13.8	13.8	6.7
4	17.5	13.3	8.7	17.5	14.5	10.9	43.7	32.6	20.5	17.5	17.6	9.2
5	21.9	16.4	10.3	21.9	18.0	13.3	54.9	40.1	24.3	21.9	22.0	10.8
6	24.8	18.0	12.3	24.8	20.1	15.8	62.0	44.1	29.1	24.8	24.9	13.2
7	28.1	20.1	14.5	28.1	22.7	18.5	70.3	49.0	34.3	28.1	28.3	15.8
8	31.9	22.7	15.2	31.9	25.7	20.1	79.7	55.2	35.6	31.9	32.1	16.0
9	35.1	24.6	17.4	35.1	28.1	22.7	87.7	59.6	40.7	35.1	35.3	18.5
10	38.1	26.4	19.5	38.1	30.5	25.3	95.3	63.9	45.0	38.1	38.5	21.0
Power law exponent	0.885 ± 0.009	0.795 ± 0.012	0.854 ± 0.022	0.885 ± 0.009	0.828 ± 0.011	0.901 ± 0.012	0.883 ± 0.010	0.785 ± 0.012	0.847 ± 0.023	0.885 ± 0.009	0.889 ± 0.009	0.863 ± 0.024

Table 4

Exponents in the power laws that describe how parameters scale with planetary mass in our models.

Variable	Definition	Power-Law Exponent
R_C	Radius of the core	$a = 0.234 \pm 0.003$
k_M	Thermal conductivity of the lower mantle	$b = 0.47 \pm 0.04$
ρ_M	Density of the lower mantle	$c = 0.23 \pm 0.01$
g	Gravitational acceleration near the core-mantle boundary	$d = 0.53 \pm 0.01$
α_M	Thermal expansivity of the lower mantle	$e = -0.69 \pm 0.03$
κ_M	Thermal diffusivity of the lower mantle	$f = 0.25 \pm 0.04$
μ_{BL}	Average viscosity in the lower mantle boundary layer	$g = 0.05 \pm 0.07$
ΔT_{BL}	Thermal contrast across the lower mantle boundary layer	$h = 0.57 \pm 0.02$
Q_{CMB}	Heat flow across the core-mantle boundary	1.56 ± 0.06

AGU PUBLICATIONS

Journal of Geophysical Research: Planets

Supporting Information for

Energetic Requirements for Dynamos in the Metallic Cores of Super-Earth and Super-Venus Exoplanets

C. H. Blaske[1,2], J. G. O'Rourke[2]

[1]Barrett, The Honors College, Arizona State University, Tempe AZ

[2]School of Earth and Space Exploration, Arizona State University, Tempe AZ

Contents of this file

Text S1.

S1.1. The Energy Budget for the Core

The energy budget for the core can be defined using a series of polynomials, which we compile here. Similar equations are presented elsewhere with different notation and some differences in the included terms (Labrosse, 2015; O'Rourke, 2020). First, the adiabatic temperature profile in the core is

$$T_a(r) = T_0\left[1-\left(\frac{r}{L_\rho}\right)^2 - A_\rho\left(\frac{r}{L_\rho}\right)^4\right]^\gamma, \qquad (S1)$$

where γ is the Grüneisen parameter (Table 2) and T_0 is the adiabatic temperature at the center of the core. If the core is entirely liquid, then T_0 is the actual temperature at r = 0 m. If an inner core exists, then T_0 is the adiabatic temperature profile in the outer core projected downwards to the center of the planet. With or without an inner core, the analytic equations for the energy budget of the outer core are derived by integrating combinations of the temperature and density profiles (Eq. 5 and S1) over the volume of the outer core. To write those expressions, we use four useful functions:

$$f_c(x,\delta) = x^3\left[1-\frac{3}{5}(\delta+1)x^2 - \frac{3}{14}(\delta+1)\left(2A_\rho-\delta\right)x^4\right], \qquad (S2)$$

$$f_k(x) = 0.2x^5\left[1+\frac{10}{7}\left(1+2A_\rho\right)x^2+\frac{5}{9}\left(3+10A_\rho+4A_\rho^2\right)x^4\right], \qquad (S3)$$

$$f_\chi(x) = x^3\left\{-\frac{1}{3}\left(\frac{R_I}{L_\rho}\right)^2+\frac{1}{2}\left[1+\left(\frac{R_I}{L_\rho}\right)^2\right]x^2-\frac{13}{70}x^4\right\}, \qquad (S4)$$

and

$$f_\gamma(x) = x^3\left[-\frac{\Gamma}{3}+\left(\frac{1+\Gamma}{5}\right)x^2+\left(\frac{A_\rho\Gamma-1.3}{7}\right)x^4\right], \qquad (S5)$$

where

$$\Gamma = \left(\frac{R_C}{L_\rho}\right)^2\left[1-\frac{1}{3}\left(\frac{R_C}{L_\rho}\right)^2\right]. \qquad (S6)$$

Most of the energetic terms are written as products of the cooling rate of the core (dT_C/dt) and polynomials that are functions of the radial structure and thermodynamic properties of the outer core. In other words, for each individual Q_i,

$$Q_i = \tilde{Q}_i\left(\frac{dT_C}{dt}\right). \qquad (S7)$$

Based on the complete energy budget for the core (Eq. 6), the overall cooling rate is

$$\frac{dT_C}{dt} = \frac{Q_{CMB} - Q_R}{\tilde{Q}_S + \tilde{Q}_P + \tilde{Q}_G + \tilde{Q}_L + \tilde{Q}_I} \, . \tag{S8}$$

If Q_{CMB} is specified as a boundary condition, we can self-consistently calculate the rest of the energy budget along with the cooling rate of the core (dT_C/dt) and, if applicable, the growth rate of the inner core (dR_I/dt). We then calculate the total dissipation available for a dynamo (Φ) using the procedure described in the main text.

Before the inner core nucleates, there are only three sources of energy in the core. First, we consider heat associated with secular cooling (i.e., the changing total thermal energy) of the core:

$$\tilde{Q}_S = -\frac{4}{3}\pi\rho_0 C_C L_\rho^3 f_c\left(\frac{R_C}{L_\rho},\gamma\right)\left[1-\left(\frac{R_C}{L_\rho}\right)^2 - A_\rho\left(\frac{R_C}{L_\rho}\right)^4\right]^{-\gamma} , \tag{S9}$$

where C_C = 750 J/kg is the specific heat of the core. Second, the total radiogenic heating in the core is

$$Q_R = M_C H_K [K] \exp(-\lambda_K t) \, , \tag{S10}$$

where $H_K = 4.2 \times 10^{-14}$ W/kg/ppm is the initial radiogenic heat production per unit mass per ppm of potassium and $\lambda_K = 1.76 \times 10^{-17}$ s^{-1} is the decay constant for potassium-40. In this study, we use t = 4.5 Gyr for this equation. In other words, the radiogenic heat production from a certain amount of potassium (e.g., specified by [K]) is benchmarked to the decay rate at present day for Earth. Finally, the precipitation of light elements at the CMB releases gravitational energy as

$$\tilde{Q}_P = \frac{8}{3}\pi G \rho_0^2 L_\rho^5 \alpha_P P_C \left[f_\gamma\left(\frac{R_C}{L_\rho}\right) - f_\gamma\left(\frac{R_I}{L_\rho}\right)\right], \tag{S11}$$

where α_P = 0.80 is the coefficient of compositional expansion associated with adding the precipitate (a combination of MgO, SiO_2, and/or FeO) to the iron alloy.

The energy budget becomes more complicated once the inner core starts growing. First, we need to replace Eq. S9 with another equation for secular cooling:

$$\tilde{Q}_S = -\frac{4}{3}\pi\rho_0 C_C L_\rho^3 \left[1-\left(\frac{R_I}{L_\rho}\right)^2 - A_\rho\left(\frac{R_I}{L_\rho}\right)^4\right]^{-\gamma} \left[\frac{dT_L}{dR_I} + \frac{2\gamma T_L(R_I)\left(\frac{R_I}{L_\rho^2}\right)\left(1+2A_\rho\left(\frac{R_I}{L_\rho}\right)^2\right)}{1-\left(\frac{R_I}{L_\rho}\right)^2 - A_\rho\left(\frac{R_I}{L_\rho}\right)^4}\right]\left[f_c\left(\frac{R_C}{L_\rho},\gamma\right) - f_c\left(\frac{R_I}{L_\rho},\gamma\right)\right]\left(\frac{dR_I}{dT_C}\right). \tag{S12}$$

Here $T_L(r_I)$ is the liquidus temperature at the inner core boundary:

$$T_L(r_I) = T_L(0) - K_0\left(\frac{dT_L}{dP}\right)\left(\frac{R_I}{L_\rho}\right)^2 + \frac{c_0}{f_c\left(\frac{R_C}{L_\rho},0\right)}\left(\frac{dT_L}{dc}\right)\left(\frac{R_I}{L_\rho}\right)^3, \qquad (S13)$$

where c_0 = 0.056 is the effective mass fraction of the light component in the core that is excluded into the outer core during inner core growth, which could represent multiple light elements. The slope of the liquidus at the inner core boundary is thus

$$\frac{dT_L}{dR_I} = -2K_0\left(\frac{dT_L}{dP}\right)\left(\frac{R_I}{L_\rho^2}\right) + \frac{3c_0}{f_c\left(\frac{R_C}{L_\rho},0\right)}\left(\frac{dT_L}{dc}\right)\left(\frac{R_I^2}{L_\rho^3}\right). \qquad (S14)$$

We compare the slopes of the liquidus and adiabat to obtain the growth rate of the inner core as the outer core cools (e.g., Nimmo 2015):

$$\frac{dR_I}{dT_C} = -\frac{1}{\left(\frac{dT_L}{dP} - \frac{dT_a}{dP}\right)_{R_I}}\left(\frac{T_L(R_I)}{T_C\rho_I g_I}\right), \qquad (S15)$$

Finally, we compute the three energetic terms related to the inner core itself. Excluding light elements from the inner core releases gravitational energy:

$$\tilde{Q}_G = \frac{8\pi^2 G\rho_0 c_0 \alpha_I R_I^2 L_p^2}{f_c\left(\frac{R_C}{L_\rho},0\right)}\left[f_\chi\left(\frac{R_C}{L_\rho}\right) - f_\chi\left(\frac{R_I}{L_\rho}\right)\right]\left(\frac{dR_I}{dT_C}\right), \qquad (S16)$$

where α_I = 0.83 is the coefficient of compositional expansion associated with the light elements released from the inner core. Next, freezing the core releases latent heat:

$$\tilde{Q}_L = 4\pi r_I^2 \rho_I T_L(R_I)\Delta S_C\left(\frac{dR_I}{dT_C}\right), \qquad (S17)$$

where ΔS_C = 127 J/K/kg is the entropy of melting for the core. We assume that the inner core is a perfect thermal conductor, meaning that its temperature everywhere equals the temperature at the inner core boundary. The associated heat flow into the outer core is

$$\tilde{Q}_I = C_C M_I K_0\left(\frac{dT_L}{dP}\right)\left(\frac{2R_I}{L_\rho^2} + \frac{16R_I}{5L_\rho^5}\right)\left(\frac{dR_I}{dT_C}\right), \qquad (S18)$$

where M_I is the mass of the inner core:

$$M_I(R_I) = \frac{4}{3}\pi\rho_0 L_\rho^3 f_c\left(\frac{R_I}{L_\rho},0\right). \qquad (S19)$$

S1.2. The Dissipation Budget for the Core

A dynamo may exist if the total dissipation calculated from the energy and entropy budgets is positive. That is, positive dissipation means that enough thermal and chemical energy is available to create mechanical energy via convection. The dynamo process is then presumed to transform mechanical energy into electromagnetic energy. We calculate the total dissipation using Eqs. 7–9 in the main text. Using the polynomial functions, we can define the average temperature in the outer core (T_D) and the effective temperature associated with dissipation from secular cooling (T_S):

$$T_D = \frac{T(R_I)}{\left[1 - \left(\frac{R_I}{L_\rho}\right)^2 - A_\rho \left(\frac{R_I}{L_\rho}\right)^4\right]^\gamma} \left[\frac{f_c\left(\frac{R_C}{L_\rho}, 0\right) - f_c\left(\frac{R_I}{L_\rho}, 0\right)}{f_c\left(\frac{R_C}{L_\rho}, -\gamma\right) - f_c\left(\frac{R_I}{L_\rho}, -\gamma\right)}\right], \qquad (S20)$$

and

$$T_S = \frac{T(R_I)}{\left[1 - \left(\frac{R_I}{L_\rho}\right)^2 - A_\rho \left(\frac{R_I}{L_\rho}\right)^4\right]^\gamma} \left[\frac{f_c\left(\frac{R_C}{L_\rho}, \gamma\right) - f_c\left(\frac{R_I}{L_\rho}, \gamma\right)}{f_c\left(\frac{R_C}{L_\rho}, 0\right) - f_c\left(\frac{R_I}{L_\rho}, 0\right)}\right]. \qquad (S21)$$

Finally, here is the equation for the dissipation sink associated with thermal conduction:

$$\Phi_K = 16\pi\gamma^2 k_C L_\rho \left[f_k\left(\frac{R_C}{L_\rho}\right) - f_k\left(\frac{R_I}{L_\rho}\right)\right] T_D. \qquad (S22)$$

Critically, we do not explicitly model any depth-dependence of the thermal conductivity. Instead, we use a constant thermal conductivity for the entire outer core but test multiple values that cover for any uncertainty related to the depth-dependence of thermal conductivity. Understanding the depth-dependence would be important to quantifying the extent of thermal stratification in the uppermost core that develops if Q_{CMB} is sub-adiabatic. However, we can assess whether a dynamo may exist without modeling in detail stratification in the outer core. In the main text, we defined the adiabatic heat flow (Eq. 10) and qualitatively described the critical heat flow for a dynamo in the presence (Q_{yesIC}) and absence (Q_{noIC}) of an inner core. The full equation for Q_{noIC} is

$$Q_{noIC} = \frac{\left(\frac{T_S}{T_D}\right)\Phi_K + \left(\frac{T_S}{T_D} - \frac{\tilde{Q}_S}{\tilde{Q}_S + \tilde{Q}_P}\right) Q_R}{\frac{T_S}{T_C} - \frac{\tilde{Q}_S}{\tilde{Q}_S + \tilde{Q}_P}}. \qquad (S23)$$

We numerically solve for Q_{yesIC} by computing Φ over a range of Q_{CMB} and finding the value of Q_{CMB} for which $\Phi \sim 0$ W. Writing an analytic equation for Q_{yesIC} is very complex.

M_P (M_E)	k_M (W/m/K)	ρ_M (kg/m^3)	μ_{BL} / $\mu_{BL}(M_E)$	T_{melt} (K)	T_{LM} (K)	$T_C(0)$ (K)	T_{BL} (K)	ΔT_{BL} (K)
1	9	5872	1.00	5000	2635	4089	3362	1454
2	11	6547	1.41	6797	3159	5474	4316	2316
3	13	7110	1.56	8243	3589	6579	5084	2990
4	15	7602	1.64	9480	3981	7528	5755	3547
5	17	8038	1.57	10555	4353	8346	6349	3993
6	20	8441	1.46	11537	4711	9085	6898	4374
7	22	8808	1.40	12423	5060	9765	7412	4705
8	24	9155	1.32	13251	5402	10399	7900	4997
9	26	9481	1.25	14021	5739	10994	8366	5255
10	27	9788	1.22	14743	6070	11560	8815	5490

Table S1. Values of various physical parameters used to calculate the power-law exponents reported in Table 4, including the thermal conductivity of the lower mantle (k_M), the density of the lower mantle (ρ_M), the average viscosity in the thermal boundary layer ratioed to that for an Earth-mass planet ($\mu_{BL}/\mu_{BL}[M_E]$), the melting temperature of silicates in the lower mantle (T_{melt}), the temperature of the lower mantle extrapolated from the potential temperature along an adiabatic gradient (T_{LM}), the temperature at the top of the core when the inner core first nucleates ($T_C[0]$), the average temperature in the boundary layer (T_{BL}) and the thermal contrast across the boundary layer in the lower mantle (ΔT_{BL}). The main text explains how each of these parameters were determined. Figure S6 shows the power laws that were fit to these values.

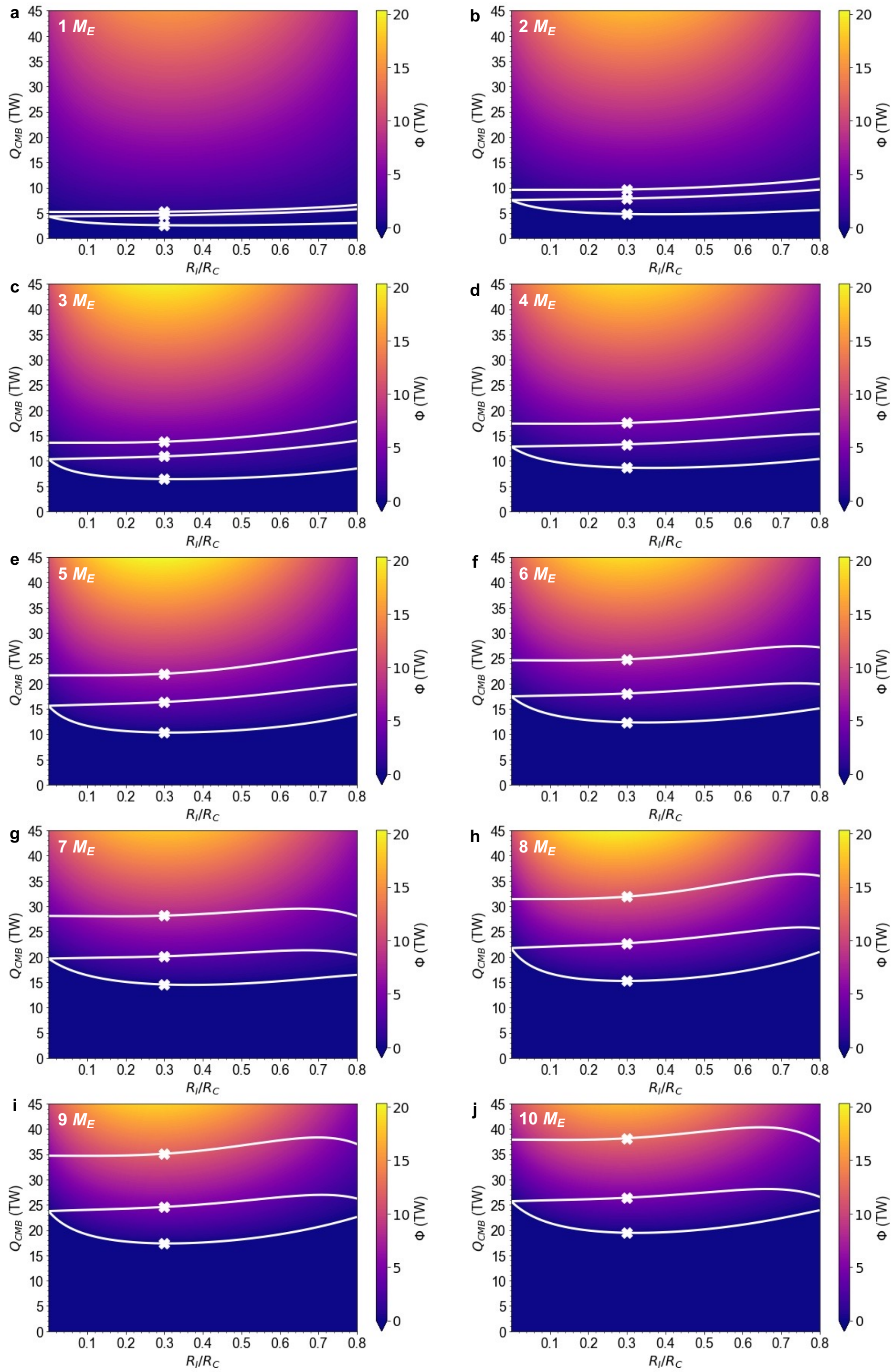

Figure S1. Heat flow required for a dynamo versus the fractional (normalized) radius of the inner core using the nominal values for [K], P_P, and k_C that are listed in Table 3. Panels (a), (e), and (j) here are identical to panels (b), (c), and (d) from Figure 3 in the main text. Other panels here show the energy regime diagrams for different planetary masses (i.e., 1–10 M_E in increments of 1 M_E). In each panel, the white curves represent Q_{ad}, Q_{noIC}, and Q_{yesIC} from top to bottom. Cross marks show the represented values at R_I/R_E ~ 0.3 that we extracted for Table 3 and to calculate the scaling laws.

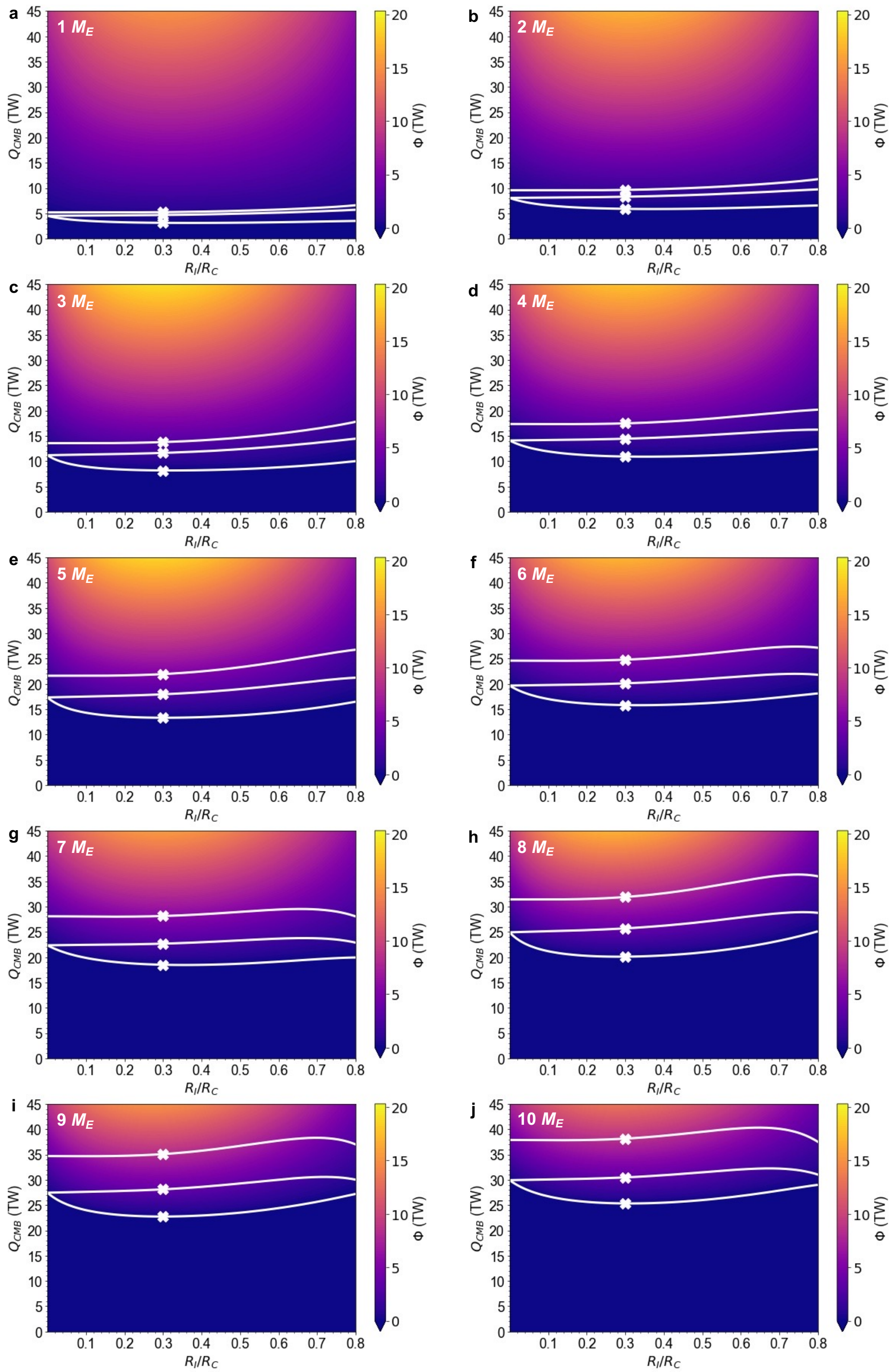

Figure S2. Same as Figure S1, except using the second set of parameters from Table 3 (i.e., [K] = 200 ppm, $P_P = 5 \times 10^{-6}$ K^{-1}, and k_C = 40 W/m/K) to explore the effects of radiogenic heating on the energetic requirements for a dynamo. In each subplot, the white curves represent Q_{ad}, Q_{noIC}, and Q_{yesIC} from top to bottom.

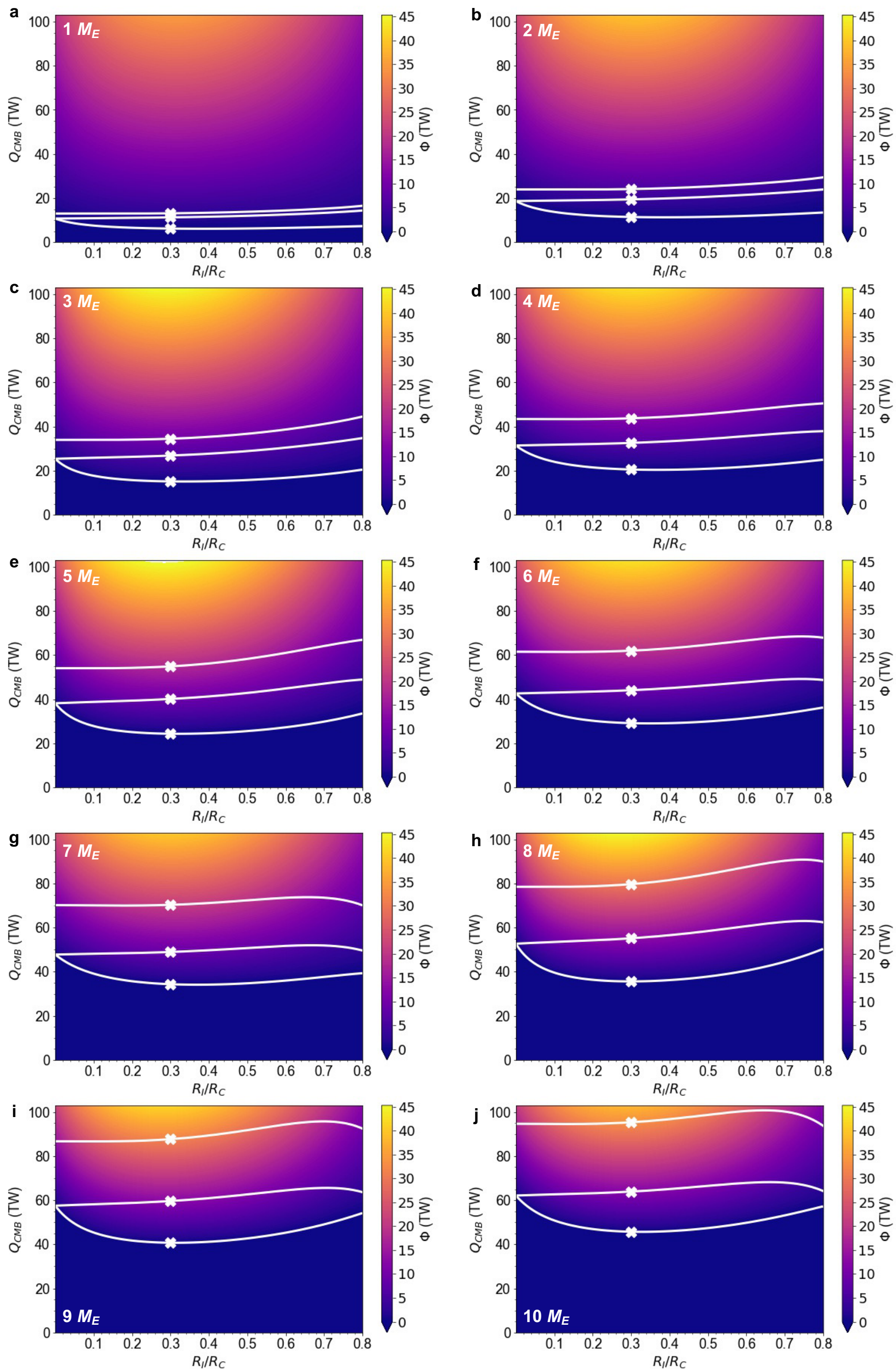

Figure S3. Same as Figure S1, except using the third set of parameters from Table 3 (i.e., [K] = 50 ppm, $P_P = 5 \times 10^{-6}$ K^{-1}, and k_C = 100 W/m/K) to explore the effects of thermal conductivity on the energetic requirements for a dynamo.

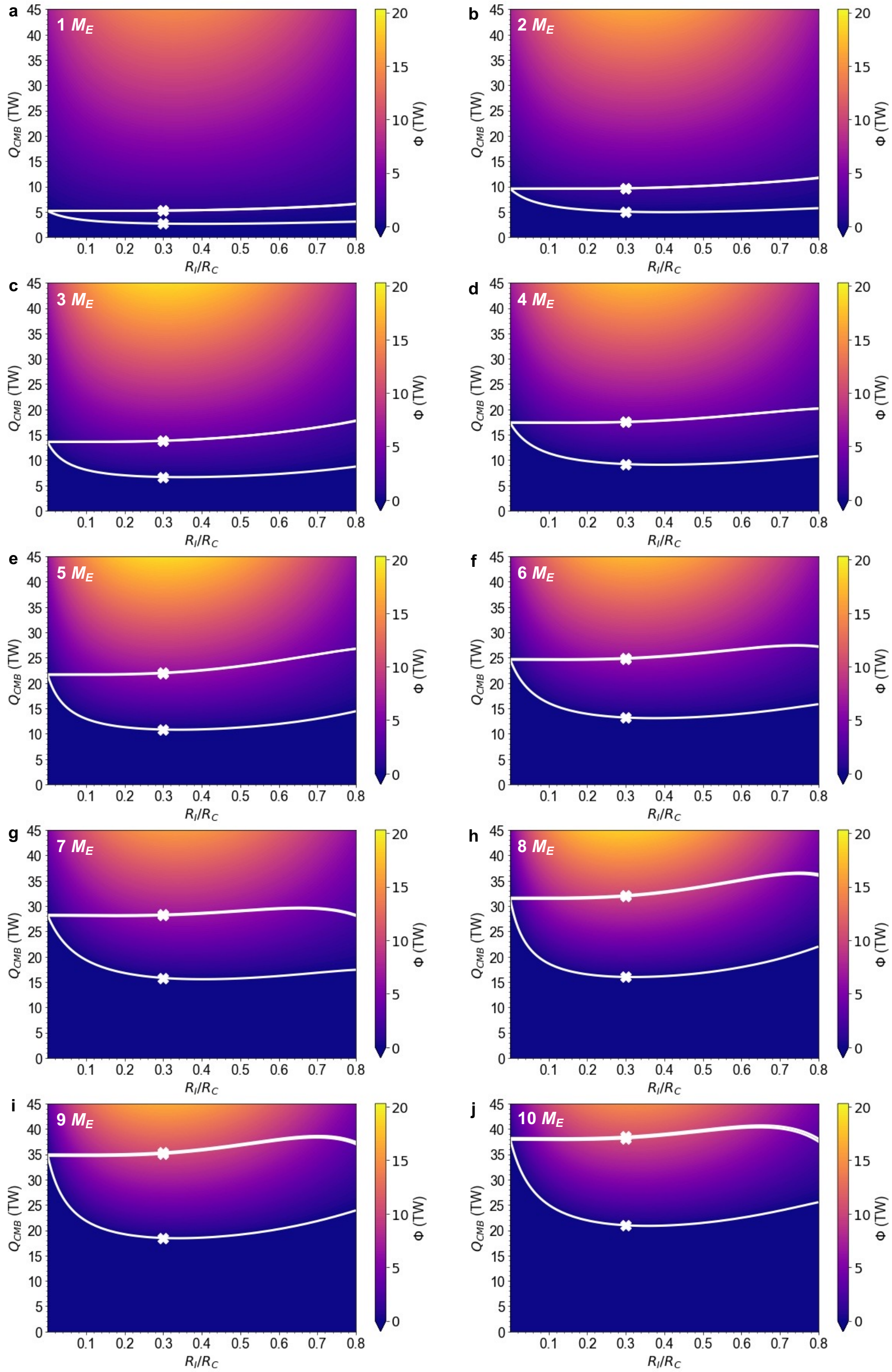

Figure S4. Same as Figure S1, except using the fourth set of parameters from Table 3 (i.e., [K] = 50 ppm, P_P = 0 K^{-1}, and k_C = 40 W/m/K) to explore the effects of the precipitation of light elements from the core at the core-mantle boundary on the energetic requirements for a dynamo. Note that Q_{ad} and Q_{noIC} are virtually identical at the scale of these plots in the absence of precipitation because radiogenic heating is small.

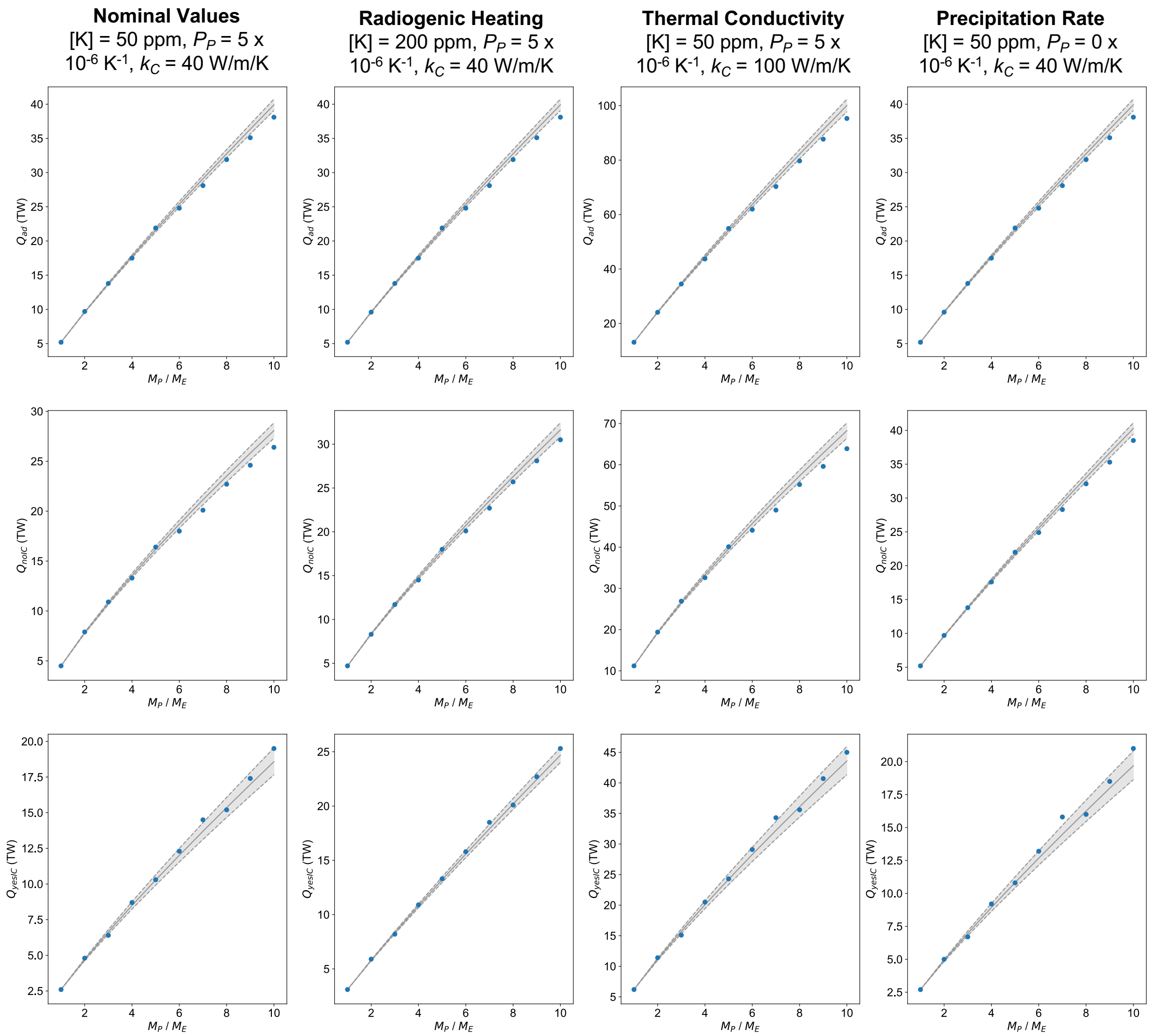

Figure S5. Power laws provide useful descriptions of how the energetic requirements for a dynamo change with planetary mass. Here we plot the representative values for Q_{ad} (top row), Q_{noIC} (middle row), and Q_{yesIC} (bottom row) that are listed in Table 3. Grey curves and shadings show the best-fit power laws and their formal errors.

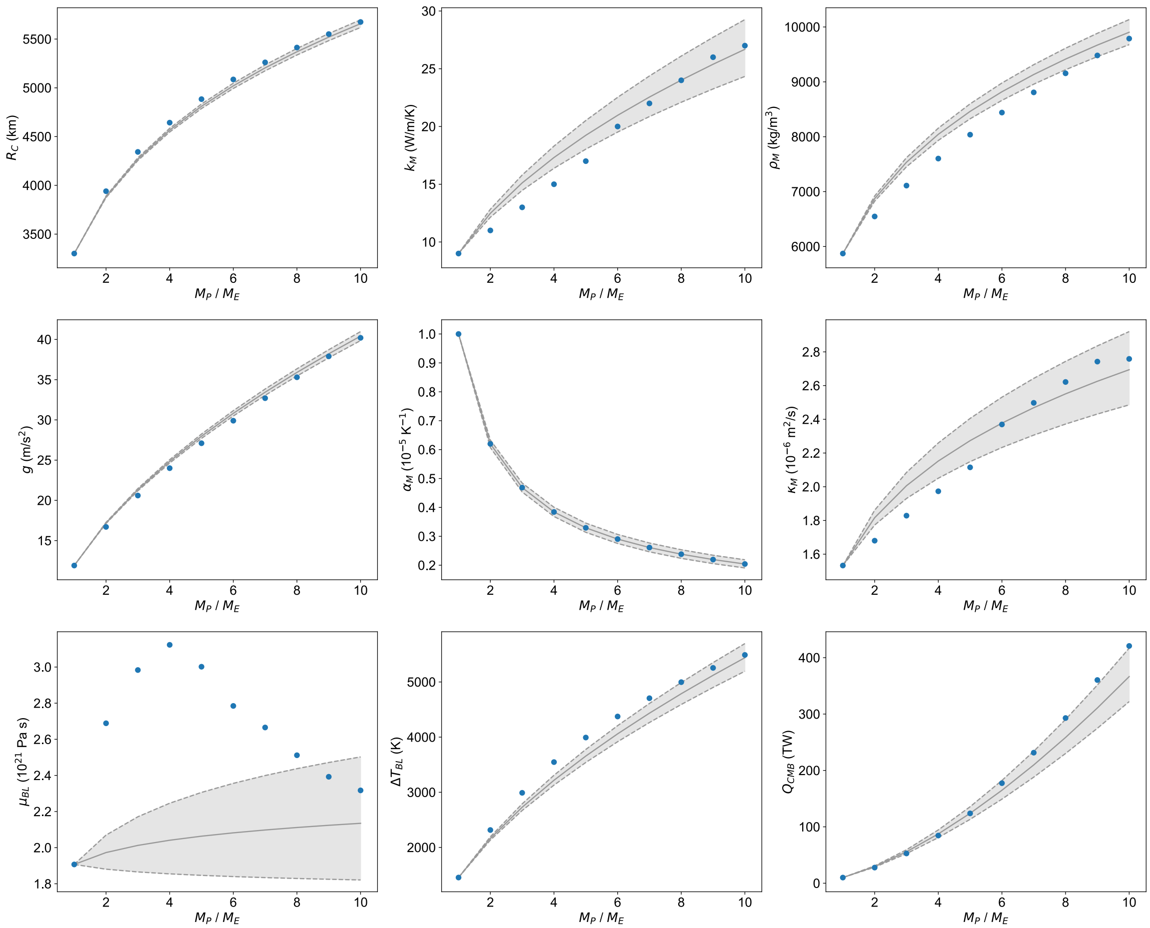

Figure S6. How the heat flow across the core-mantle boundary changes with planetary mass is well-described using a power law, even though one parameter does not follow a power-law relationship. Each subplot showcases a different parameter used to formulate the scaling law for Q_{CMB} in the main text. Blue dots are the values from Table S1. Grey lines and shadings show the best-fit power laws and their formal errors that are listed in Table 4. All parameters and Q_{CMB} are adequately fit except for the mantle viscosity (μ_{BL}), which is intrinsically uncertain in any case.